

# Distributed Motion Planning for Safe Autonomous Vehicle Overtaking via Artificial Potential Field

Songtao Xie, *Student Member, IEEE*, Junyan Hu, *Member, IEEE*, Parijat Bhowmick, *Member, IEEE*, Zhengtao Ding, *Senior Member, IEEE*, and Farshad Arvin, *Senior Member, IEEE*

**Abstract**—Autonomous driving of multi-lane vehicle platoons have attracted significant attention in recent years due to their potential to enhance the traffic-carrying capacity of the roads and produce better safety for drivers and passengers. This paper proposes a distributed motion planning algorithm to ensure safe overtaking of autonomous vehicles in a dynamic environment using the Artificial Potential Field method. Unlike the conventional overtaking techniques, autonomous driving strategies can be used to implement safe overtaking via formation control of unmanned vehicles in a complex vehicle platoon in the presence of human-operated vehicles. Firstly, we formulate the overtaking problem of a group of autonomous vehicles into a multi-target tracking problem, where the targets are dynamic. To model a multi-vehicle system consisting of both autonomous and human-operated vehicles, we introduce the notion of velocity difference potential field and acceleration difference potential field. We then analyze the stability of the multi-lane vehicle platoon and propose an optimization-based algorithm for solving the overtaking problem by placing a dynamic target in the traditional artificial potential field. A simulation case study has been performed to verify the feasibility and effectiveness of the proposed distributed motion control strategy for safe overtaking in a multi-lane vehicle platoon.

**Index Terms**—Motion planning, intelligent vehicles, artificial potential field, autonomous overtaking, collision avoidance, distributed systems.

## I. INTRODUCTION

As the number of private cars and rented vehicles increases rapidly in all countries, traffic congestion, road safety and environmental pollution are becoming critical issues [1]. The autonomous driving and vehicle platooning strategies offer potential and realistic solutions to these challenges [2], [3]. In addition to reducing human-caused traffic accidents [4], autonomous driving and vehicle platooning may result in better fuel economy [5], reduced traffic congestion [6], improved traffic efficiency [7] and reduced environmental pollution. Extensive research has been done on autonomous vehicle's perception, decision-making, motion control, motion planning, and traffic scheduling [8]–[12]. The current research

This work was supported by EU H2020-FET-OPEN RoboRoyale project [grant number 964492].

S. Xie and Z. Ding are with the Department of Electrical and Electronic Engineering, The University of Manchester, Manchester, M13 9PL, UK. (e-mails: {songtao.xie, zhengtao.ding}@manchester.ac.uk)

J. Hu is with the Department of Computer Science, University College London, London, WC1E 6BT, UK. (e-mail: junyan.hu@ucl.ac.uk)

P. Bhowmick is with the Department of Electronics and Electrical Engineering, Indian Institute of Technology Guwahati, Guwahati, 781039, India (e-mail: parijat.bhowmick@iitg.ac.in)

F. Arvin is with the Swarm & Computational Intelligence Laboratory (SwalCIL), Department of Computer Science, Durham University, UK. (e-mail: farshad.arvin@durham.ac.uk)

trend, however, focuses mainly on the self-driving mechanism of single-lane platoons. However, in the case of multi-lane platoons, the vehicles may face conflicting situations while operating at high speed and overtaking other vehicles due to a lack of communication among the vehicles of the different lanes. This hence affects both traffic safety and efficiency of a large vehicle platoon.

With the advent of heterogeneous vehicle platooning techniques, self-driving scheme has significantly improved the carrying capacity of the lanes and the road safety [13]. Information exchange and sharing, collaborative sensing, joint operation of the multi-vehicle system ensure the possibility of cooperation among intelligent vehicles, thus improving the overall driving quality and driving safety [14], [15]. For instance, V2X communication in a multi-agent system connects vehicles with the network of road facility agents. It enables information exchange and coordinated operation among vehicle agents, which significantly reduces traffic congestion in complex roads [7]. A multi-vehicle system can also achieve a specific formation, i.e., maintain the desired distance between neighboring vehicles, increasing road capacity, reducing congestion, and improving traffic efficiency [16], [17]. Moreover, a multi-vehicle system may bring more positive possibilities for road rescue, traffic command and other fields [18]. Despite all these positive factors, no automotive companies have yet deployed autonomous multi-vehicle scheme into practical use.

In recent years, much progress has been made in the study of multi-vehicle systems, which includes unmanned vehicle formations [19], [20], cooperative navigation of unmanned vehicles [21], and multi-vehicle merging [22], [23]. Among them, the cooperative adaptive cruise control of vehicles is more relevant and will greatly improve the efficiency of existing traffics. However, many research works on such multi-vehicle platoon systems are still limited to the control of vehicle motion in a single dimension, i.e., only the longitudinal motion of the platoon can be controlled. This technique may not fulfill the requirements in most real world applications as longitudinal motion control alone cannot deal with the situation when there exist vehicles blocking the road. Therefore, to handle unexpected scenarios in the road, safe autonomous overtaking methods should be considered in the protocol design of autonomous vehicles (AVs).

One of the most typical application scenarios of AVs is the overtaking of multi-vehicle system in a dynamic environment in which obstacles and vehicles have varying accelerations. The multi-vehicle system's overtaking is a highly complex scenario, including various traffic scenarios, such as lane

changing, obstacle avoidance, formation, and target tracking. The overtaking of autonomous driving has always been a challenging research topic. In [24]–[29], overtaking decisions, planning, and control have all been studied in depth. Motion planning is an integral part of the overtaking problem which provides a state trajectory with time series for obstacle avoidance, lane changing and overtaking [30]. Model predictive control (MPC) plays a vital role in motion planning [24], [31], [32]. All of these methods transform motion planning into a finite-time quadratic programming problem. Thus, a trajectory satisfying the specific constraints is obtained [33]. Then, using some optimization techniques, a smoother motion trajectory can be obtained [34]. Besides, the graph search-based method [8], sampling-based method [35], and interpolation curve method [36] are also used in motion planning for overtaking scenarios of autonomous vehicles. Moreover, reinforcement learning also provides a potential solution to the overtaking behavior of autonomous driving [37]–[39]. Deep deterministic strategy gradient method and deep Q-learning network become the mainstream algorithm frameworks [40], [41]. However, these studies of overtaking motion planning are all based on a single vehicle system.

There are fewer research works on the motion planning of the overtaking application of the autonomous multi-vehicle system. The article [42] proposed an advanced graph-based optimal solution for overtaking scenarios of multi-vehicles. On this basis, [43] proposed another method of automatic vehicle overtaking based on MPC. The graph optimization algorithm based on that probability provides the path of obstacle avoidance and overtaking. In [44], a unified approach to cooperative path-planning based on nonlinear model predictive control was proposed for overtaking application of multi-vehicle systems. Subsequently, the trajectory prediction of the human driver model was integrated into the framework, such that the behaviors of the other agents were affected by the human-operated vehicles (HVs) [45]. In [46], a distributed control method for coordinating multiple vehicles in the framework of an automated valet parking system was introduced. The main limitation of this approach is to rely on traffic infrastructure, which poses a considerable challenge to the current traffic facilities. The work presented in [47] proposed an integrated route and motion planning approach by considering a set of customer demands and road rules specified in temporal logic. However, vehicles other than navigators cannot interact with other existing vehicles during the overtaking.

This paper proposes a distributed multi-vehicle motion planning method motivated by the challenges mentioned above in multi-vehicle overtaking. The method presented in this paper is to transform the overtaking of the automatic driving fleet into multiple dynamic target tracking problems by assigning a virtual dynamic target for the leader of fleet. Firstly, a safe and feasible trajectory is planned for the leader AV so as to achieve tracking of the dynamic virtual target and obstacle avoidance of the HVs and other AV fleet members. To solve a dynamic target tracking problem, this paper introduces the artificial potential field to carry out the motion planning of target tracking. The position field, velocity field and acceleration field are added between the leader AV and the dynamic virtual target to

realize the accurate tracking of the virtual target by the leader AV. Simultaneously, the position and speed repulsion fields are added between the leader AV, the HVs, and other AV fleet members to realize the cooperative collision avoidance among the AV fleet members and avoid the HVs in the environment. Secondly, we design a bounded distributed control protocol that can guarantee topology connectivity for the followers. By using this distributed control protocol, the followers can track the leader AV with varying acceleration. Meanwhile, followers can also achieve obstacle avoidance with HVs, road boundaries, and other AV fleet members, and achieve distance stabilization between followers. By introducing velocity and acceleration fields to achieve overtaking of dynamic HV, the Artificial Potential Field (APF) method, which is widely used for motion planning of a single mobile robot, can be applied to solve the overtaking motion planning problem of multi-vehicle systems. Furthermore, we introduce a bounded distributed control protocol that achieves speed consistency across the AV fleet and avoids collisions among the vehicles. To the best of authors' knowledge, such a APF-based motion planning strategy has not been proposed in the literature.

The main contributions of this paper can be summarized as follow:

- A distributed motion planning algorithm for the leader AV based on the improved artificial potential field is proposed, which enables the leader AV to complete the overtaking of dynamic human-operated vehicles.
- We design a bounded distributed control protocol to implement the follower's safe tracking of the leader AV. Moreover, we analyze the stability of the multi-vehicle system with  $N$  followers and one leader AV. It is proved that under this control protocol, the velocity of all the followers will be synchronized with the leader AV, and all the AVs will keep a safe distance between them.
- The effectiveness of the proposed strategy for use in autonomous vehicle overtaking scenario is validated by a realistic simulator, Unreal Engine™.

## II. PROBLEM STATEMENT

We consider using the following double integral dynamical system kinematics equation to approximate the motion of the  $N$  vehicles in a 2D space:

$$\begin{cases} \dot{r}_i = v_i \\ \dot{v}_i = a_i \end{cases} \quad (1)$$

where  $r_i \in \mathbb{R}^2$ ,  $v_i \in \mathbb{R}^2$  are, respectively, the position, velocity vector of vehicle  $i$ . We use a time-varying directed graph  $G(t) \triangleq (\mathcal{V}, \mathcal{E}(t))$  to describe the network topology between vehicles. where  $\mathcal{V} \triangleq \{\mathcal{V}_1, \dots, \mathcal{V}_N\}$  is set of nodes. and elements of  $\mathcal{E}(t) \in N \times N$  are denoted as  $(\mathcal{V}_i, \mathcal{V}_j)$  which is termed an edge from  $\mathcal{V}_i$  to  $\mathcal{V}_j$ .  $A(t) = [a_{ij}] \in \mathbb{R}^{N \times N}$  is the adjacency matrix of graph  $G(t)$ . The initial connection of the system is:  $\mathcal{E}(0) = \{(i, j) | \|r_i(0) - r_j(0)\| < \rho_c, i, j \in \mathcal{V}\}$ , where  $\rho_c$  is the communication range of the vehicles.

The AV fleet overtaking scenario can be summarized as a dynamic multi-target tracking problem. We assume that the AV

fleet consists of  $N$  followers and 1 leader AV. With Vehicle-to-Vehicle (V2V) communication technology [48], vehicle terminals exchange real-time state information directly with each other without the need for forwarding through a base station. AVs need to avoid other HVs actively in the environment; meanwhile, the AVs also need to avoid collisions between each other. We consider setting up one dynamic virtual node which represent the target position. The motion parameters of the virtual node need to be determined according to the HVs. The virtual node should always be in front of the HVs and have the same velocity and acceleration parameters as the HVs. Therefore, overtaking task can be decoupled into three tasks. Firstly, in a limited time, the leader AV must reach the virtual node. Secondly, the followers in the AV fleet must remain synchronous in the motion parameters with the leader AV. Thirdly, all the AVs must avoid HVs and avoid collisions with members of the AV fleet.

#### A. Basic Assumptions

- We assume that it takes time  $\tau$  ( $\tau > 0$ ) seconds for the platoon system to switch the connection topology each time.
- In the current environment, there are  $N + 1$  AVs and  $M$  human-operated vehicles. Human-operated vehicles appear randomly in the environment.
- The V2V communication function allows vehicles to communicate their position, velocity, and acceleration with each other. The communication range is limited. When other vehicles enter the communication range of vehicle  $i$ , vehicle  $i$  can receive the status information of adjacent vehicles.
- During the overtaking, all vehicles are connected by a communication network. The communication network topology is shown in Fig. 1. The communication range of each AV is  $\rho_c$ . We assume that the initial topology  $G(0)$  is connected. The communication between AVs is bidirectional, where AVs can access state information from each other. Note that HVs do not communicate with other vehicles and each HV's state information is obtained by the on-board sensors of nearby AVs. Since the delays and errors can be minimized by the high-performance sensors, this information flow can also be viewed as a unidirectional communication system for analytical purposes, where AVs can access state information from HVs, but HVs will not use any information from AVs.
- Without loss of generality, we assume that each HV has a changing acceleration. The jerk of the vehicle is constant,  $\ddot{r} = J$ .
- Because of the differences in traffic laws between countries and regions, we assume that it is legal to overtake on the left and the right.

#### B. A specific scenario

In this paper, we use the specific scenario shown in Fig. 2 to carry out the experiments. Fig. 2 depicts a two-lane overtaking scene of an AV fleet, where H1 denotes the human-operated vehicle, L1, F1, and F2, respectively, denote the leader AV, first follower AV, and second follower AV.

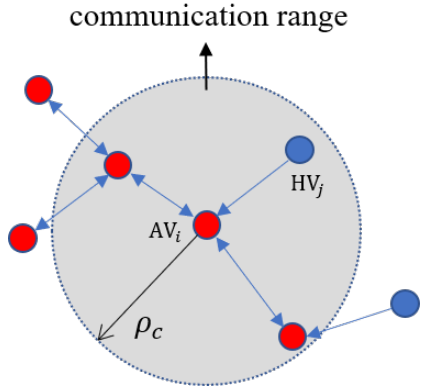


Fig. 1: The communication network amongst the autonomous vehicles (indicated by Red circles) and human-operated vehicles (indicated by Blue circles).

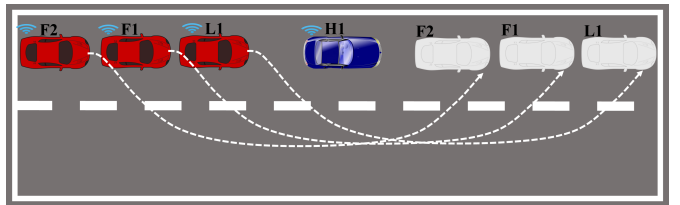


Fig. 2: A typical overtaking scenario of autonomous vehicles. H1 denotes the human-operated vehicle, L1, F1, and F2, respectively, denote the leader AV, first follower AV, and second follower AV.

vehicle, L1, F1, and F2, respectively, denote the leader AV, first follower AV, and second follower AV. Red cars are AVs in a particular formation; blue car is the object to be overtaken, grey cars represent the desired position of autonomous vehicles fleet after overtaking. We consider the most common overtaking scenario, in which the AV fleet changes lanes to overtake, then needs to make a second lane change and return to the initial lane. In this scenario, the road is a two-lane straight road segment, and each lane has a fixed width. Additionally, the human-operated vehicle's acceleration in front of the AV fleet is continuously changing during overtaking.

#### C. System architecture of automatic driving

This paper assumes that each AV fleet member has the most commonly used autonomous driving system architecture, making this paper's method feasible in real autonomous vehicles. Fig. 3 describes a general system architecture of automatic driving function. The planning module will generate a position trajectory with a time sequence in each control cycle. The control module will track this trajectory accurately. Motion Planning aims to plan a safe, comfortable, and derivable trajectory for an autonomous vehicle according to the data from the prediction, perception, localization, high definition map (HD-Map) and routing module. In this paper, The AV fleet members can obtain the position, velocity, and acceleration of human-operated vehicles and the other AV fleet members through the perception module. The prediction module will

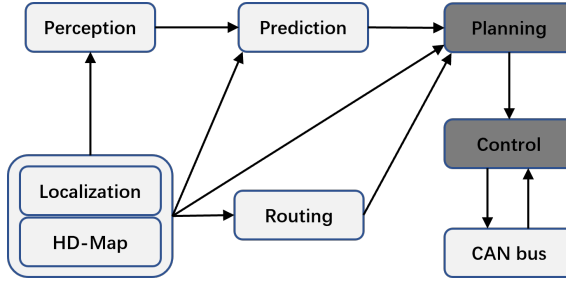


Fig. 3: Functional block diagram of an intelligent autopilot scheme for autonomous vehicles.

predict the driving intention, position and velocity changes of the human-operated vehicles and output the human-operated vehicle's predictive motion trajectory in the finite time domain. In traditional single-vehicle autonomous driving, motion planning during overtaking considers the environment vehicles and achieve overtaking and lane changing. While in multi-vehicle autonomous driving, motion planning should also take into account the risk of collisions between AV fleet members and the specific formation requirements of the AV fleet. The main objective of this paper is to develop algorithms in planning and control blocks to achieve safe overtaking behaviors of the AV fleet. This AV fleet constitutes a typical distributed system. All individual agents in this distributed system are isomorphic autonomous vehicles and use the same autonomous driving system architecture shown in Fig. 3.

### III. DISTRIBUTED MOTION PLANNING AND CONTROL DESIGN

#### A. Motion planning of the navigator

The idea of using artificial potential field method for path planning has a long history. The basic idea comes from the concept of potential in physics. The obstacles in the environment generate repulsive force to the robot, the target points generate attraction to the robot, and the robot moves along the direction of minimum potential energy under the resultant force's action. The artificial potential field method is often applied in path planning and multi-agent motion control in recent years [24]. The advantage of this method is that it is simple to calculate and easy to realize real-time control. The traditional artificial potential field method is based on the distance difference between the robot and the target or obstacle to generate the corresponding attractive and repulsive forces. Following functions generate a typical attractive potential field and repulsive potential field [49]:

$$\begin{cases} U_{\text{att}} = \frac{1}{2} K_p d^2(r) \\ F_{\text{att}} = -\nabla U_{\text{att}}(r) \end{cases} \quad (2)$$

and

$$\begin{cases} U_{\text{rep}} = \frac{1}{2} \eta_p \left( \frac{1}{d(r)} - \frac{1}{D} \right)^2 \\ F_{\text{rep}} = -\nabla U_{\text{rep}}(r) \end{cases} \quad (3)$$

However, the traditional APF technique is mostly used for path planning in a static environment and may not be effective in

a dynamic environment. Hence, it is necessary to modify the traditional APF technique relying on the positional difference.

Let there be  $M$  human-operated vehicles in the current scenario. The current position of the leader AV, the  $k^{\text{th}}$  AV, the  $j^{\text{th}}$  HV, and the goal position of leader AV are denoted by  $r_l$ ,  $r_k$ ,  $r_j$  and  $r_g$  respectively. Similarly, the velocities and accelerations are denoted by  $v_l$ ,  $v_k$ ,  $v_j$ ,  $v_g$  and  $a_l$ ,  $a_k$ ,  $a_j$ ,  $a_g$ , respectively. In addition, we define the following variables:

- $d(r_l, r_k)$  is the geometric distance between the leader AV and the  $k^{\text{th}}$  AV. The relative velocity and relative acceleration between the leader AV and the  $k^{\text{th}}$  AV in the fleet are symbolized as  $d(v_l, v_k)$  and  $d(a_l, a_k)$ ;
- $d(r_l, r_j)$  is the geometric distance between the leader AV and the  $j^{\text{th}}$  HV. The relative velocity and relative acceleration between the leader AV and the  $j^{\text{th}}$  HV are symbolized as  $d(v_l, v_j)$  and  $d(a_l, a_j)$ ;
- $d(r_l, r_g)$  is the geometric distance between the leader AV and the goal node. The modulus of relative velocity and relative acceleration between the leader AV and the goal node are denoted by  $d(v_l, v_g)$ , and  $d(a_l, a_g)$ .

Hence, the goal node of leader AV is given by the routing block when the decision-making level makes the decision to overtake. This dynamic goal node will change with the state of motion of the HV.

In order to achieve the leader AV's tracking of the virtual target, we define the following artificial potential field.

1) *Attractive Quadratic Potential Fields*: We define the following Attractive Quadratic Potential Field (AQPF)

$$U_{\text{att}}(r, v, a) = \frac{1}{2} K_p d^2(r_l, r_g) + \frac{1}{2} K_v d^2(v_l, v_g) + \frac{1}{2} K_a d^2(a_l, a_g) \quad (4)$$

between the leader autonomous vehicle and the virtual goal (treated as a node). The attractive force produced by the proposed AQPF technique is given by

$$\begin{aligned} F_{\text{att}}(i) &= -\nabla U_{\text{att}}(r, v, a) \\ &= -\frac{\partial U_{\text{att}}(r, v, a)}{\partial r} - \frac{\partial U_{\text{att}}(r, v, a)}{\partial v} - \frac{\partial U_{\text{att}}(r, v, a)}{\partial a} \\ &= -K_p d(r_l, r_g) - K_v d(v_l, v_g) - K_a d(a_l, a_g) \\ &= F_{\text{attP}} + F_{\text{attV}} + F_{\text{atta}}, \end{aligned} \quad (5)$$

where  $K_p > 0$ ,  $K_v > 0$  and  $K_a > 0$  denote respectively the position, velocity, and acceleration gain coefficients. Fig. 4 shows the vector diagram for calculating the attractive force between an leader AV and its goal node. The  $F_{\text{attP}}$  aims to make the autonomous vehicle track the position of the goal node. The direction of the force is from the leader AV to the goal node. The  $F_{\text{attV}}$  aims to make the leader AV track the velocity of the goal node, and its direction is the same as the direction of vector  $(\vec{v}_g - \vec{v}_l)$ . The  $F_{\text{atta}}$  aims to complete the acceleration tracking, and its direction is the same as the direction of vector  $(\vec{a}_g - \vec{a}_l)$ .

2) *Repulsive Potential Field generated by the HVs*: Regarding the potential field of HVs, we also consider the potential field caused by position and speed. The distance

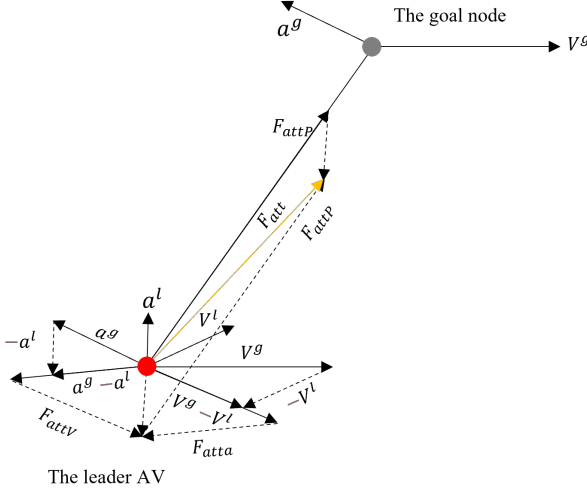


Fig. 4: The vector diagram has been used for calculating the attractive force between the leader AV (red circle) and the its goal node (grey circle).

factor ensures that an autonomous vehicle will not collide with HVs. The speed factor can predict and avoid collisions in advance. We define  $\vec{d}(v_l, v_j)$  and  $\vec{d}(r_l, r_j)$  the relative velocity and position vectors of the leader and the HVs. When  $\vec{d}(v_l, v_j) \cdot \vec{d}(r_l, r_j) > 0$ , it means that the leader AV will have the risk of collision with the HVs, thus the HVs generate the repulsive force to the leader AV. Hence, we establish the following repulsive potential field:

$$U_{\text{rep}(lj)(r,v)} = \begin{cases} \frac{1}{2}\eta_p \left( \frac{1}{d(r_l, r_j)} - \frac{1}{D_{\max}} \right)^2 d(r_l, r_g) + \eta_v d(v_l, v_j), \\ \frac{1}{2}\eta_p \left( \frac{1}{d(r_l, r_j)} - \frac{1}{D_{\max}} \right)^2 d(r_l, r_g), \\ 0; \end{cases} \quad (6)$$

for

$$\begin{cases} d(r_j, r_l) \leq D_{\max} \text{ and } \vec{d}(v_l, v_j) \cdot \vec{d}(r_l, r_j) > 0; \\ d(r_l, r_j) \leq D_{\max} \text{ and } \vec{d}(v_l, v_j) \cdot \vec{d}(r_l, r_j) \leq 0; \\ d(r_l, r_j) > D_{\max}. \end{cases}$$

where  $D_{\max}$  denotes the repulsive area defined by the following elliptical equation:

$$\frac{(x - x_j)^2}{a^2} + \frac{(y - y_j)^2}{b^2} = 1 \quad (\text{where } a > b > 0). \quad (7)$$

The elliptical action area allows the vehicle to avoid obstacles in advance in the longitudinal direction. The region  $D_{\max}$  defined by formula (7) is a variable value.

$$D_{\max} = \sqrt{\frac{a^2 b^2 (1 + k^2)}{b^2 + a^2 k^2}}, \quad (8)$$

where  $k = \frac{y_i - y_j}{x_i - x_j}$ .

We define that the gradient of repulsive potential fields is

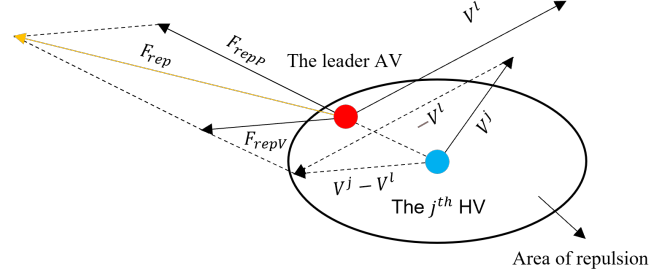


Fig. 5: Schematic diagram of repulsive force calculation between leader AV (red circle) and HV (blue circle).

the repulsive force

$$\begin{aligned} F_{\text{rep}}(lj) &= -\nabla U_{\text{rep}(lj)}(r, v) \\ &= -\frac{\partial U_{\text{rep}(lj)}(r, v)}{\partial r} - \frac{\partial U_{\text{rep}(lj)}(r, v)}{\partial v} \\ &= F_{\text{rep}P}(lj) + F_{\text{rep}V}(lj). \end{aligned} \quad (9)$$

Fig. 5 describes the calculation process of repulsive force between the leader AV and the  $j^{\text{th}}$  HV. The repulsive force  $F_{\text{rep}P}(lj)$  generated by the position difference is directed from the obstacle vehicle to the autonomous vehicle. This repulsion trend the AV away from the obstacle vehicle. The repulsive force  $F_{\text{rep}V}(lj)$  due to the velocity difference is in the same direction as the vector  $(\vec{v}_j - \vec{v}_l)$ . This repulsive force causes the autonomous vehicle to slow down when approaching an obstacle vehicle.

$$F_{\text{rep}}(lj) = \begin{cases} \eta_p \left( \frac{1}{d(r_l, r_j)} - \frac{1}{D_{\max}} \right) \frac{d(r_l, r_g)}{d^2(r_l, r_j)} \\ + \frac{1}{2}\eta_p \left( \frac{1}{d(r_l, r_j)} - \frac{1}{D_{\max}} \right)^2 + \eta_v, \\ \eta_p \left( \frac{1}{d(r_l, r_j)} - \frac{1}{D_{\max}} \right) \frac{d(r_l, r_g)}{d^2(r_l, r_j)} \\ + \frac{1}{2}\eta_p \left( \frac{1}{d(r_l, r_j)} - \frac{1}{D_{\max}} \right)^2, \\ 0, \end{cases} \quad (10)$$

for

$$\begin{cases} d(r_j, r_l) \leq D_{\max} \text{ and } \vec{d}(v_l, v_j) \cdot \vec{d}(r_l, r_j) > 0; \\ d(r_l, r_j) \leq D_{\max} \text{ and } \vec{d}(v_l, v_j) \cdot \vec{d}(r_l, r_j) \leq 0; \\ d(r_l, r_j) > D_{\max}. \end{cases}$$

Hence, the total repulsive force of human-operated vehicles to the leader AV is:

$$F_{\text{rep}j}(l) = \sum_{j=1}^M F_{\text{rep}}(lj). \quad (11)$$

*3) Repulsive Potential Field generated by the autonomous vehicles:* For the overtaking scenario in this paper, we should consider avoiding human-operated vehicles and consider collisions between members of the fleet. Similarly, the repulsion

field is defined between vehicles within the AV fleet,

$$F_{\text{rep}}(lk) = \begin{cases} \eta_p \left( \frac{1}{d(r_l, r_k)} - \frac{1}{D_{\max}} \right) \frac{d(r_l, r_g)}{d^2(r_l, r_k)} \\ + \frac{1}{2} \eta_p \left( \frac{1}{d(r_l, r_k)} - \frac{1}{D_{\max}} \right)^2 + \eta_v, \\ \eta_p \left( \frac{1}{d(r_l, r_k)} - \frac{1}{D_{\max}} \right) \frac{d(r_l, r_g)}{d^2(r_l, r_k)} \\ + \frac{1}{2} \eta_p \left( \frac{1}{d(r_l, r_k)} - \frac{1}{D_{\max}} \right)^2, \\ 0, \end{cases} \quad (12)$$

for

$$\begin{cases} d(r_l, r_k) \leq D_{\max} \text{ and } \vec{d}(v_l, v_k) \cdot \vec{d}(r_l, r_k) > 0; \\ d(r_l, r_k) \leq D_{\max} \text{ and } \vec{d}(v_l, v_k) \cdot \vec{d}(r_l, r_k) \leq 0; \\ d(r_l, r_k) > D_{\max}. \end{cases}$$

Moreover, the repulsive force calculation between the leader AV and other members in the AV fleet is the same as shown in Fig. 5. The total repulsive force exerted by the other members in the fleet on the leader AV is given by:

$$F_{\text{repk}}(l) = \sum_{k=1}^{N-1} F_{\text{rep}}(lk). \quad (13)$$

*4) Repulsive Potential Field generated due to road boundary and the resultant force calculation:* In order to make the vehicle drive within a reasonable road range, we define the potential field for the road boundary:

$$U_{\text{rep}}(\text{road}) = \begin{cases} \frac{1}{2} \eta_{\text{road}} \left( \frac{1}{d(r_l, r_{\text{road}})} - 1 \right)^2, & d(r_l, r_{\text{road}}) \leq 1; \\ 0, & d(r_l, r_{\text{road}}) > 1; \end{cases} \quad (14)$$

and

$$F_{\text{rep}}(\text{road}) = \begin{cases} \eta_{\text{road}} \left( \frac{1}{d(r_l, r_{\text{road}})} - 1 \right) \\ \times \frac{1}{d^2(r_l, r_{\text{road}})}, & d(r_l, r_{\text{road}}) \leq 1; \\ 0, & d(r_l, r_{\text{road}}) > 1, \end{cases} \quad (15)$$

where  $d(r_l, r_{\text{road}})$  represents the distance between the leader AV and road boundary.

To sum up, the resultant force of the leader AV in the environment is

$$F_{\text{total}}(l) = F_{\text{att}}(l) + F_{\text{repj}}(l) + F_{\text{repk}}(l) + F_{\text{rep}}(\text{road}). \quad (16)$$

### B. Steady-state analysis of leader AV

From the equations (10) and (12), the repulsive forces generated by an human-operated vehicle have the same form as those generated by other members of the AV fleet. Moreover, the repulsive forces generated by the road boundary exist only within a small range of the boundary, and their direction is parallel to the lateral direction. When analyzing the steady state and stability of the algorithm, we ignore this part of

repulsion. Therefore, we unify the repulsive force into the following formula, which is called the interference term:

$$Q = \sum_{f \in \mathcal{N}_l} \eta_p \left( \frac{1}{r_l - r_f} - \frac{1}{D_{\max}} \right) \frac{r_l - r_g}{(r_l - r_f)^2} \\ + \frac{1}{2} \eta_p \left( \frac{1}{r_l - r_f} - \frac{1}{D_{\max}} \right)^2 + \eta_v, \quad (17)$$

where  $r_f$  denotes the the position of vehicles which generate the repulsive force to the leader AV. Considering a particle dynamics, the following equation is obtained:

$$\ddot{r}_l = \frac{1}{m} [-K_p(r_l - r_g) - K_v(\dot{r}_l - \dot{r}_g) \\ - K_a(\ddot{r}_l - \ddot{r}_g) + Q]. \quad (18)$$

We define the difference between the position of the leader AV and the virtual dynamic node as the control object:

$$\begin{cases} e = r_l - r_g \\ \dot{e} = \dot{r}_l - \dot{r}_g \\ \ddot{e} = \ddot{r}_l - \ddot{r}_g \\ \dddot{e} = \dddot{r}_l - \dddot{r}_g. \end{cases} \quad (19)$$

The closed loop dynamic model is updated to:

$$\ddot{e} = \frac{1}{m} [-K_p e - K_v \dot{e} - K_a \ddot{e} \\ + \sum_{f \in \mathcal{N}_l} \eta_p \left( \frac{1}{e + r_g - r_f} - \frac{1}{D_{\max}} \right) \frac{e}{(e + r_g - r_f)^2} \\ + \frac{1}{2} \eta_p \left( \frac{1}{e + r_g - r_f} - \frac{1}{D_{\max}} \right)^2 + \eta_v] - \ddot{r}_g. \quad (20)$$

Defining  $B_f := r_g - r_f$  and the following equation can be obtained:

$$\ddot{e} = \frac{1}{m} [-K_p e - K_v \dot{e} - K_a \ddot{e} \\ + \sum_{f \in \mathcal{N}_l} \eta_p \left( \frac{1}{e + B_f} - \frac{1}{D_{\max}} \right) \frac{e}{(e + B_f)^2} \\ + \frac{1}{2} \eta_p \left( \frac{1}{e + B_f} - \frac{1}{D_{\max}} \right)^2 + \eta_v] - \ddot{r}_g. \quad (21)$$

The equilibrium state of system is obtained by setting  $\ddot{e} = \dot{e} = 0$ , which results in the following equations:

$$\frac{1}{m} [-K_p e + \sum_{f \in \mathcal{N}_l} \eta_p \left( \frac{1}{e + B_f} - \frac{1}{D_{\max}} \right) \frac{e}{(e + B_f)^2} \\ + \frac{1}{2} \eta_p \left( \frac{1}{e + B_f} - \frac{1}{D_{\max}} \right)^2 + \eta_v] - \ddot{r}_g = 0. \quad (22)$$

The solution is as follows:

$$e = F(B_1, B_2, \dots, B_f, \ddot{r}_g). \quad (23)$$

Whether there are variables  $B_f$  depends on whether the vehicle is subject to interference item.  $f$  is the number of obstacles vehicles and other fleet members which are generating repulsive force to the leader AV. Variable  $\ddot{r}_g$  is the jerk of

the virtual target. Therefore, one of the necessary conditions for the steady state of the system is that  $\ddot{r}_g$  is constant. This is consistent with our previous basic assumption that dynamic virtual targets have varying accelerations. In general, in the case of small changes in acceleration, we can think about jerk as zero. Therefore, the steady state of the system under the disturbance term depends on the value of  $B_f$ . Therefore, when  $B_f$  is also constant, the system is purely in steady state. In this case, the vehicle is likely to enter a local steady state formed by  $B_f$ , which prevents tracking of the virtual target node. Its steady state value is given in (23). However, this does not meet our requirements when modeling the overtaking problem. We expect that the vehicle will not enter a steady state when approaching the obstacle. To solve this problem, we randomly add noise  $w_f$  to the repulsive force field of obstacles, so that the vehicle will not enter a steady state:

$$\begin{aligned} \ddot{e} = & \frac{1}{m}[-K_p e - K_v \dot{e} - K_a \ddot{e} \\ & + \sum_{f \in \mathcal{N}_l} \eta_p \left( \frac{1}{e + r_g - r_f} - \frac{1}{D_{\max}} \right) \frac{e}{(e + r_g - r_f)^2} \\ & + \frac{1}{2} \eta_p \left( \frac{1}{e + r_g - r_f} - \frac{1}{D_{\max}} \right)^2 + \eta_v + w_f] - \ddot{r}_g. \end{aligned} \quad (24)$$

In addition, the addition of random noise follows the following rule:

$$\begin{cases} w_f = 0 & \text{if } \mathcal{N}_l = \emptyset \\ w_f \neq 0 & \text{if } \mathcal{N}_l \neq \emptyset \end{cases}. \quad (25)$$

Then (23) is updated to:

$$e = F(B_1, B_2, \dots, B_f, w_f, \ddot{r}_g). \quad (26)$$

When the vehicle is affected by the interference term, it will not enter the steady state because of the noise  $w_f$ , but will leave the repulsive region because of the repulsive force. The vehicle will then enter a attractive field with no interference terms. Essentially, according to (25),  $w_f$  will be eliminated when the vehicle is not affected by the interference term. Thus, when the vehicle converges to the steady state without disturbance terms, (24) is then updated to:

$$\ddot{e} = \frac{1}{m}[-K_p e - K_v \dot{e} - K_a \ddot{e}] - \ddot{r}_g. \quad (27)$$

The steady state can be solved by the following equation:

$$\ddot{r}_g + \frac{1}{m} K_p e = 0. \quad (28)$$

The set of equilibrium states  $\mathbb{E}$  is therefore obtained as

$$\mathbb{E} = \left\{ \ddot{e}, \dot{e}, e \mid e = -\frac{m \ddot{r}_g}{K_p}, \ddot{e} = \dot{e} = 0 \right\}. \quad (29)$$

According to the above analysis, the velocity and acceleration parameters of leader AV will converge to those of the virtual target, and its position will converge to  $(r_g - \frac{m \ddot{r}_g}{K_p})$ .

Relying on the above analysis, we can conclude that an autonomous vehicle can dynamically track a virtual target following the proposed algorithm. However, the vehicle cannot

completely converge to the position of the virtual target. There exist a positional difference between the them, the value of which depends on the jerk of the virtual target  $\ddot{r}_g$  and the constant parameters  $K_p, m$ . Therefore, the algorithm is suitable for a dynamic target with a small jerk. However, this algorithm is not useful for the dynamic targets whose acceleration varies significantly. In a real-world scenario, due to the unpredictable road conditions, obstacles and nonuniformities of the vehicles, different driving styles of the human drivers lead to frequent acceleration changes. Hence, the previous algorithm needs to be modified to enable a vehicle to track unforeseen circumstances (modelled as dynamic targets/obstacles) during the course of motion. In order to eliminate the influence of the jerk of the target node on the steady-state error of the position, we consider introducing the jerk of the target node into the closed-loop control:

$$\begin{aligned} F_{\text{att}}(l) = & -K_p \left( r_l - r_g - \frac{m \ddot{r}_g}{K_p} \right) - K_v (\dot{r}_l - \dot{r}_g) \\ & - K_a (\ddot{r}_l - \ddot{r}_g). \end{aligned} \quad (30)$$

We will now use the same analysis to obtain the third-order system model of an autonomous vehicle as follows:

$$\begin{aligned} \ddot{e} = & \frac{1}{m} \left[ -K_p \left( e - \frac{m \ddot{r}_g}{K_p} \right) - K_v \dot{e} - K_a \ddot{e} \right. \\ & + \sum_{f \in \mathcal{N}_l} \eta_p \left( \frac{1}{e + r_g - r_f} - \frac{1}{D_{\max}} \right) \frac{e}{(e + r_g - r_f)^2} \\ & \left. + \frac{1}{2} \eta_p \left( \frac{1}{e + r_g - r_f} - \frac{1}{D_{\max}} \right)^2 + \eta_v + w_f \right] - \ddot{r}_g. \end{aligned} \quad (31)$$

Without being affected by the interference term, the state space expression of the closed-loop control system can be expressed as

$$\begin{bmatrix} \dot{e} \\ \ddot{e} \\ \ddot{r}_g \end{bmatrix} = \begin{bmatrix} 0 & 1 & 0 \\ 0 & 0 & 1 \\ -\frac{K_p}{m} & -\frac{K_v}{m} & -\frac{K_a}{m} \end{bmatrix} \begin{bmatrix} e \\ \dot{e} \\ \ddot{e} \end{bmatrix}. \quad (32)$$

The set of steady-state operating points of the above system is obtained as

$$\mathbb{E} = \{ \ddot{e}, \dot{e}, e \mid \ddot{e} = \dot{e} = e = 0 \}. \quad (33)$$

The set  $\mathbb{E}$  signifies that the position, velocity and acceleration of leader AV converges to the motion parameters corresponding to the virtual target. Stability of closed-loop control systems can be determined by  $A$  matrix, where

$$A = \begin{bmatrix} 0 & 1 & 0 \\ 0 & 0 & 1 \\ -\frac{K_p}{m} & -\frac{K_v}{m} & -\frac{K_a}{m} \end{bmatrix}. \quad (34)$$

Let  $|\lambda E - A| = 0$ , Characteristic equation is:

$$\lambda^3 + \frac{K_a}{m} \lambda^2 + \frac{K_v}{m} \lambda + \frac{K_p}{m} = 0, \quad (35)$$

where  $\frac{K_p}{m} > 0, \frac{K_v}{m} > 0, \frac{K_a}{m} > 0$ . It's easy to conclude that the characteristic equation has no solution greater than or equal to zero. Therefore, the matrix  $A$  must be negative definite or semi-negative definite. In conclusion, the closed-loop control

system is Lyapunov stable or Lyapunov asymptotically stable.

### C. Trajectory generation and optimization

1) *Trajectory generation:* On the premise of not affecting the algorithm itself, we consider using a particle dynamics model for trajectory prediction. Select state vector  $S$ :

$$S_l = \begin{bmatrix} r_l \\ v_l \\ a_l \end{bmatrix}, \quad (36)$$

and equation of state for the system:

$$\dot{S}_l = AS_l + BU_l, \quad (37)$$

where,

$$A = \begin{bmatrix} 0 & 1 & 0 \\ 0 & 0 & 1 \\ 0 & 0 & 0 \end{bmatrix}, \quad B = \begin{bmatrix} 0 \\ 0 \\ \frac{1}{m} \end{bmatrix}.$$

Use the forward Euler method to discretize the equation of state:

$$\dot{S}_l \approx \frac{S_l(t+1) - S_l(t)}{T} = AS_l(t) + BU_l(t), \quad (38)$$

where  $T$  is the control period. The equation of state after discretization is

$$S_l(t+1) = (I + TA)S_l(t) + TBU_l(t) = \bar{A}S_l(t) + \bar{B}U_l(t), \quad (39)$$

where

$$\bar{A} = \begin{bmatrix} 1 & T & 0 \\ 0 & 1 & T \\ 0 & 0 & 1 \end{bmatrix}, \quad \bar{B} = \begin{bmatrix} 0 \\ 0 \\ \frac{T}{m} \end{bmatrix}.$$

In the finite time domain, the predicted trajectory and state of the vehicle can be obtained by:

$$U_l(t) = mJ_g(t) - K_p(r_l(t) - r_g(t)) - K_v(v_l(t) - v_g(t)) - K_a(a_l(t) - a_g(t)), \quad (40)$$

where  $J_g(t)$  is the jerk of target node.  $U_l(t)$  is a discrete-time signal where  $t = 0, 1, 2, \dots$  denotes the discrete time instants.

In addition, the traffic speed limit and the power limit of the vehicle are also taken into account. The acceleration and velocity constraints are defined as

$$a_l(t+1) = \begin{cases} a_l(t) + \frac{T}{m}U_l(t), & \left| a_l(t) + \frac{T}{m}U_l(t) \right| < a_{\max} \\ a_{\max}, & \left| a_l(t) + \frac{T}{m}U_l(t) \right| \geq a_{\max} \end{cases} \quad (41)$$

and

$$v_l(t+1) = \begin{cases} v_l(t) + Ta_l(t), & |v_l(t) + Ta_l(t)| < v_{\max} \\ v_{\max}, & |v_l(t) + Ta_l(t)| \geq v_{\max} \end{cases}. \quad (42)$$

2) *Trajectory optimization:* The trajectory generated by the APF technique satisfies the vehicle's barrier avoidance constraints and the motion tracking of the target point. However, the resulting trajectory does not guarantee sufficient smoothness in the event of curvature changes and acceleration changes. In the literature, there are a variety of local trajectory

optimization techniques. For instance, the idea of optimal control for local rolling optimization is often considered. In the longitudinal direction, to minimize the jerk and thereby increasing the passengers' comfort, the following optimization problem

$$\min_{j_x(t)} J_x = \int_t^{t+q} \frac{1}{2} j_x^2(t) dt \quad (43)$$

such that  $\dot{x}(t) = v_x(t), \dot{v}_x(t) = a_x(t), \dot{a}_x(t) = j_x(t)$ .

can be solved taking the inspiration from [50]. According to Pontryagin's maximum principle, the optimal longitudinal displacement trajectory  $x(t)$  can be obtained. In (43), the position constraint must be added to meet the obstacle avoidance requirements. Meanwhile, the velocity and acceleration constraints at the endpoints needs to be introduced to ensure the smoothness of the generated trajectories. Similarly, in the lateral direction, the objection function is established as followed [50]:

$$\min_{j_y(t)} J_y = \int_t^{t+q} \frac{1}{2} j_y^2(t) dt \quad (44)$$

such that  $\dot{y}(t) = v_y(t), \dot{v}_y(t) = a_y(t), \dot{a}_y(t) = j_y(t)$ .

The two optimal problems above end up with two high-order curves, which ensures the requirement of avoiding obstacles and the smoothness of the acceleration change.

Another local optimization method, high-order Bessel curve fitting [51], is also adopted in this paper. It can obtain locally smoother trajectories but may not obtain the optimal solution. We consider using the fifth-order Bessel curve to carry out rolling optimization on the obtained trajectory to obtain a trajectory that is as smooth as possible in the finite time domain.

Given  $(n+1)$  space vectors  $P_i \in R^3$ , where  $i \in \{0, 1, 2, \dots, n\}$ , the  $n$ -th Bessel curve can be defined as

$$P(t) = \sum_{i=0}^n P_i B_i^n(t) \quad \forall t \in [0, 1], \quad (45)$$

where  $P_i$  are the control points and  $B_i^n(t)$  is given by:

$$B_i^n(t) = C_n^i t^i (1-t)^{n-i} \quad \forall i \in \{0, 1, \dots, n\}. \quad (46)$$

The fifth-order Bessel curve has a very smooth curvature and the corresponding changes in the turning angle and angular velocity are relatively gentle. In the terminology of vehicular control, this signifies that the curvature of turning of a vehicle will be smoother.

3) *Motion planning algorithm:* After the decision of overtaking is made by the leader AV of multi-vehicle system, the leader needs to generate virtual target node. Virtual target node are generated according to Algorithm 1. Let  $S_j = [r_j, v_j, a_j]^T$  and  $S_g = [r_g, v_g, a_g]^T \in R^3$  represent the state vector of the  $j^{th}$  HV and the goal node, respectively. Note that this static coupling can be described as  $S_g = S_j + \Delta d$ , where  $\Delta d = [C + \mu, 0, 0]^T$ ,  $C$  is the platoon length and  $\mu$  is the desired distance between HV and the platoon.  $S_l(p)$  in this algorithm represents the leader AV's state vector at time step  $p$ , which include position, velocity and acceleration. In the actual self-driving vehicle, the motion planning needs to be updated

in real-time and sent to the control module. Algorithm 2 provides a reference trajectory for the leader AV to avoid the dynamic vehicle. The algorithm is updated dynamically in real-time, each update calculates the motion trajectory in the finite time domain.

---

**Algorithm 1** Virtual target node generation algorithm

---

**Input:** The current state variables of autonomous vehicle fleet members, human-operated vehicles  $S_l(p)$ ,  $S_j(p)$ . Prediction state of human-operated vehicles in  $p$  time domain,  $S_j(p)$ ,  $S_j(p+1)$ ,  $\dots$ ,  $S_j(p+q)$ .

**Output:** The target node's lane number  $L_g$  and the target node's motion parameters  $S_g$ .

- 1: Initialize basic parameters, control period  $T$ , and prediction time domain  $q$ .
  - 2: **for** each control cycle.
  - 3: Leader AV receives the lane number of itself,  $L_l$ .
  - 4: Leader AV receives the predictive states  $S_j(p+1)$ ,  $\dots$ ,  $S_j(p+q)$  from prediction module.
  - 5: Find vehicle  $HV_g$  with  $\max(S_j)$ .
  - 6:  $L_g = L_l$ ;
  - 7:  $S_g = \max(S_j) + \Delta d$ .
  - 8: Leader AV calculates the state of the virtual target node in proactive time domain.
  - 9: **End for**
  - 10: **Return**  $S_g(p)$ ,  $S_g(p+1)$ ,  $\dots$ ,  $S_g(p+q)$ .
- 

**Algorithm 2** Overtaking motion planning algorithm for autonomous vehicles in a dynamic environment

---

**Input:** The current state variables of leader AV, human-operated vehicles, and, goal node,  $S_l(p)$ ,  $S_j(p)$ ,  $S_g(p)$ . Prediction state of human-operated vehicles and goal nodes in  $p$  time domain,  $S_j(p)$ ,  $S_j(p+1)$ ,  $\dots$ ,  $S_j(p+q)$ ,  $S_g(p)$ ,  $S_g(p+1)$ ,  $\dots$ ,  $S_g(p+q)$ .

**Output:**  $S_l(p)$ ,  $S_l(p+1)$ ,  $\dots$ ,  $S_l(p+q)$ .

- 1: Initialize basic parameters, control period  $T$ , and prediction time domain  $q$ .
  - 2: **While**  $|d(S_l(p), S_g(p))| >$  threshold value
  - 3: Receive the current position and velocity  $S_l(p)$ ,  $S_g(p)$ .
  - 4: Receive the predictive states  $S_j(p+1)$ ,  $\dots$ ,  $S_j(p+q)$  from prediction module.
  - 5: **For** each predictive time sequence  $\in q$ 
    - 6: Calculate the artificial potential force  $U_l(p)$ .
    - 7: Calculate and save the next state  $S_l(p+1)$  of autonomous vehicle relying on (39).
  - 8: **End for**
  - 9: **Return**  $S_l(p)$ ,  $S_l(p+1)$ ,  $\dots$ ,  $S_l(p+q)$ .
  - 10: Use the high-order Bessel curve for trajectory optimization based on (45). Or use optimal control for trajectory optimization based on (43) and (44).
  - 11: Send the optimized trajectory sequence  $S_l(p)$ ,  $S_l(p+1)$ ,  $\dots$ ,  $S_l(p+q)$  to control module.
  - 12: **End while**
- 

**D. Distributed control protocol for followers**

In practical applications, due to the large size of the vehicle structure, we expect that the vehicle can achieve one-to-one following, which is more conducive to the AV fleet to overtake on the road with limited width, and will not occupy too much road resources. Hence, we define a new control connection topology  $\mathcal{G}(t) = (\bar{\mathcal{V}}, \bar{\mathcal{E}}(t))$ .  $\bar{A}(t) = [\bar{a}_{ij}] \in \mathbb{R}^{N \times N}$  is the adjacency matrix of graph  $\mathcal{G}(t)$ . Define for each  $i$  node a neighbor:

$$\bar{\mathcal{N}}_i = \left\{ j \in N : \|r_i(t) - r_j(t)\| \leq R_j, \min \|r_i(t) - r_j(t)\|, \right. \\ \left. r_j(t) \geq r_i(t) \right\}.$$

We consider using a leader AV to guide the cluster movement of the AV fleet. Define  $r_l, v_l$  as, respectively, the position, velocity vector of leader AV. We define two classes of bounded potential field functions  $V_{ij}$ ,  $V_{il}$ ,  $V_{ik}$  and  $V_{en}$ , where  $V_{ij}$  and  $V_{il}$  are the same type of potential field function,  $V_{ik}$  and  $V_{en}$  are the other one type of potential field function.

- $V_{ij}$  is a bounded potential field function between vehicles, which mainly solve the following problems: Collision avoidance, distance stabilization, connectivity keeping.
- $V_{il}$  is the bounded potential field function between followers and leader AV, which ensures that the follower can continuously follow the leader AV.
- $V_{ik}$  is the potential field between the followers and human-operated vehicle  $k$ , which ensures there is a safe distance between AV and human-operated vehicle.
- $V_{en}$  is the potential field formed by the structured road environment, which ensures that the vehicle travels within the desired road range.

Inspired by reference [52], the control protocol we designed is as follows:

$$a_i = - \sum_{j \in \bar{\mathcal{N}}_i} \nabla_{r_i} V(\|r_{ij}\|) - h_i \nabla_{r_i} V(\|r_{il}\|) \\ - \nabla_{r_i} V(\|r_{en}\|) - \sum_{k \in \bar{\mathcal{N}}_i} \nabla_{r_i} V(\|r_{ik}\|) \\ - \alpha \sum_{j \in \bar{\mathcal{N}}_i} \bar{a}_{ij} \left\{ \text{sgn} \left[ \begin{array}{l} \sum_{p \in \bar{\mathcal{N}}_i} \bar{a}_{ip} (v_i - v_j) \\ + h_i (v_i - v_l) \end{array} \right] \right\} \\ + \alpha \sum_{j \in \bar{\mathcal{N}}_i} \bar{a}_{ij} \left\{ \text{sgn} \left[ \begin{array}{l} \sum_{p \in \bar{\mathcal{N}}_j} \bar{a}_{jp} (v_j - v_p) \\ + h_j (v_j - v_l) \end{array} \right] \right\}, \quad (47)$$

where  $h_i(t) = \begin{cases} 1 & i \in \mathcal{N}_l(t) \\ 0 & \text{others} \end{cases}$ ,  $\alpha$  is control gain.

Define a semi-positive definite energy function:

$$\begin{aligned} Q(x, v, r_l, v_l) = & \sum_{i=1}^N \left( \sum_{j \in \bar{\mathcal{N}}_i} V(\|r_{ij}\|) + h_i V(\|r_{il}\|) \right. \\ & + V(\|r_{en}\|) + \sum_{k \in \bar{\mathcal{N}}_i} V(\|r_{ik}\|) \left. \right) \\ & + \frac{1}{2} \sum_{i=1}^N (v_i - v_l)^T (v_i - v_l). \end{aligned} \quad (48)$$

Based on this energy function, we define a maximum of the energy function  $Q_{max}$ :

$$\begin{aligned} Q_{max} = & \frac{N(N-1)}{2} V_{max}(\|r_{ij}\|) + MNV_{max}(\|r_{ik}\|) \\ & + NV_{max}(\|r_{en}\|) + NV_{max}(\|r_{il}\|) \\ & + \frac{1}{2} \sum_{i=1}^N (v_i(0) - v_l(0))^T (v_i(0) - v_l(0)). \end{aligned} \quad (49)$$

In order to ensure the boundedness of the control input, realize collision avoidance, and maintain connectivity, we adopt the following interaction potential function [53]:

$$\begin{aligned} V_{ij}(\|r_{ij}\|) = & \frac{(\|r_{ij}\| - d)^2 (R_j - \|r_{ij}\|)}{\|r_{ij}\| + \frac{d^2(R_j - \|r_{ij}\|)}{c_1 + Q_{max}}} \\ & + \frac{\|r_{ij}\| (\|r_{ij}\| - d)^2}{(R_j - \|r_{ij}\|) + \frac{\|r_{ij}\|(R_j - d)^2}{c_2 + Q_{max}}}, \end{aligned} \quad (50)$$

where  $d$  is the desired distance between vehicles, and  $R_j$  is the communication range of vehicle  $j$ .

In addition, in order to ensure that the vehicle is always in the road boundary, while being able to avoid human-operated vehicles in the environment.  $V_{ik}(\|r_{ik}\|)$  and  $V_{en}(\|r_{en}\|)$  should satisfy the following conditions:  $V_{ik}(\|r_{ik}\|)$  and  $V_{en}(\|r_{en}\|)$  are continuous, differentiable, monotonically decreasing over the interval  $\|r_{ik}\|, \|r_{en}\| \in (0, d_{ek}]$ , where  $d_{ek}$  denotes the minimum distance allowed between the vehicle  $i$  and the road boundary or human-operated vehicles. Additionally, these two interaction potential fields also need to meet the following conditions:

$$\begin{aligned} V_{ik}(0) &= c_3 + Q_{max}, \\ V_{en}(0) &= c_4 + Q_{max}, \\ V_{ik}(d_{ek}) &= 0, \\ V_{en}(d_{ek}) &= 0. \end{aligned} \quad (51)$$

$V_{ik}$  and  $V_{en}$  are also potential field functions of the form (50). Their parameters will be adjusted according to the actual application. Moreover, this two interaction potential functions only work on the interval  $(0, d_{ek}]$ . This is because the human-operated vehicles and the road boundary exert only repulsive forces on the AV fleet members.

### E. Stability analysis

To consider a multi-vehicle system consisting of  $N$  follower vehicles and one leader AV, the dynamics models of both the leader AV and the followers satisfy (1), we design the

control protocol (47) for all follower vehicles. We assume that the lateral and longitudinal accelerations of all vehicles have maximum values, and  $\|\dot{v}_l\|_1 \leq a_{max}$ . When the initial connection topology  $G(0)$  is connected, and the initial energy  $Q(0)$  is limited, if the control gain  $\alpha > \frac{a_{max}}{2}$ , the connection of the whole multi-vehicle system will be kept, all followers will gradually synchronize velocity with the leader AV and achieve obstacle avoidance.

Define a position difference vector  $\tilde{r}_i = r_i - r_l$  and velocity difference vector  $\tilde{v}_i = v_i - v_l$  between the vehicle  $i$  and leader AV. We can get the following equations:

$$\begin{aligned} \dot{\tilde{r}}_i &= \tilde{v}_i \\ \dot{\tilde{v}}_i = & - \sum_{j \in \bar{\mathcal{N}}_i} \nabla_{\tilde{r}_i} V(\|r_{ij}\|) - h_i \nabla_{\tilde{r}_i} V(\|r_{il}\|) \\ & - \nabla_{\tilde{r}_i} V(\|r_{en}\|) - \sum_{k \in \bar{\mathcal{N}}_i} \nabla_{\tilde{r}_i} V(\|r_{ik}\|) - \dot{v}_l \\ & - \alpha \sum_{j \in \bar{\mathcal{N}}_i} \bar{a}_{ij} \left\{ \text{sgn} \left[ \sum_{p \in \bar{\mathcal{N}}_i} \bar{a}_{ip} (\tilde{v}_i - \tilde{v}_p) \right] \right\} \\ & + \alpha \sum_{j \in \bar{\mathcal{N}}_i} \bar{a}_{ij} \left\{ \text{sgn} \left[ \sum_{p \in \bar{\mathcal{N}}_j} \bar{a}_{jp} (\tilde{v}_j - \tilde{v}_p) \right] \right\}. \end{aligned} \quad (52)$$

Energy function (48) can be redefined as:

$$\begin{aligned} Q(\tilde{r}, \tilde{v}) = & \sum_{i=1}^N \left( \sum_{j \in \bar{\mathcal{N}}_i} V(\|r_{ij}\|) + h_i V(\|r_{il}\|) \right. \\ & + V(\|r_{en}\|) + \sum_{k \in \bar{\mathcal{N}}_i} V(\|r_{ik}\|) \left. \right) \\ & + \frac{1}{2} \sum_{i=1}^N \tilde{v}_i^T \tilde{v}_i. \end{aligned} \quad (53)$$

In the interval  $[t_0, t_1]$ , control connection topology  $\mathcal{G}(t)$  will not update. We take the first derivative of the energy function (53) with respect to time:

$$\begin{aligned} \dot{Q}(\tilde{r}, \tilde{v}) = & \sum_{i=1}^N \left( \sum_{j \in \bar{\mathcal{N}}_i} v_i \nabla_{\tilde{r}_i} V(\|r_{ij}\|) + h_i v_i \nabla_{\tilde{r}_i} V(\|r_{il}\|) \right. \\ & + v_i \nabla_{\tilde{r}_i} V(\|r_{en}\|) + \sum_{k \in \bar{\mathcal{N}}_i} v_i \nabla_{\tilde{r}_i} V(\|r_{ik}\|) \left. \right) \\ & + \sum_{i=1}^N \tilde{v}_i \dot{v}_i. \end{aligned} \quad (54)$$

Substituting (52), (55) can be obtained, where  $H(t_0) = \text{diag}\{h_1, h_2, \dots, h_N\}$ . By the definition of the Laplace matrix,  $\bar{L}(t) = \bar{D}(t) - \bar{A}(t)$ .  $\bar{D} = \text{diag}\{d_i\}$ , where  $d_i$  is the in-degree of the node  $i$ . For the control connection topology  $\mathcal{G}(t)$ ,  $\min(d_i) = 1$ . Since the initial topology of a multi-vehicle system is connected,  $\exists h_i = 1$ . Hence,  $\min \|\bar{L}(t_0) + H(t_0)\|_1 = 2$ . According to the assumption

$\alpha > \frac{a_{max}}{2}$ , Equation (55) can be transformed into:

$$\begin{aligned}\dot{Q}(\tilde{r}, \tilde{v}) &\leq (a_{max} - 2\alpha) \|\tilde{v}\|_1 \\ &\leq 0, \forall t \in [t_0, t_1].\end{aligned}\quad (56)$$

The Equation (56) indicates that  $Q(t) \leq Q(t_0) < Q_{max}, \forall t \in [t_0, t_1]$ , which means:

- The distance between vehicle  $i$  and road boundary will not be zero.
- The distance between vehicle  $i$  and human-operated vehicles will not be zero.
- the length of communication connection between vehicle  $i$  and vehicle  $j$  will not be zero and will not equal  $R_j$ .

Therefore,  $\forall t \in [t_0, t_1]$ , the vehicle will not reach the road boundary, and will not lose the communication connection with other vehicles. Meanwhile, the multi-vehicle system will not collide, nor will it collide with human-operated vehicles.

Without loss of generality, we assume that the control connection topology switches at  $t_{n-1}$ . The newly formed connection topology consists of  $N_f$  follower-follower connections, and  $N_l$  follower-leader connections. According to the definition of  $\mathcal{G}(t)$ , it follows that:

$$\begin{aligned}1 &\leq N_l \leq N \\ N-1 &\leq N_f \leq \frac{N(N-1)}{2}.\end{aligned}\quad (57)$$

Therefore,

$$\begin{aligned}Q(t_{n-1}) &\leq N_f V_{max}(\|r_{ij}\|) + MNV_{max}(\|r_{ik}\|) \\ &\quad + NV_{max}(\|r_{en}\|) + N_l V_{max}(\|r_{il}\|) \\ &\quad + \frac{1}{2} \sum_{i=1}^N (v_i(0) - v_l(0))^T (v_i(0) - v_l(0)) \\ &\leq Q_{max}.\end{aligned}\quad (58)$$

In the interval  $[t_{n-1}, t_n]$ , taking the first derivative of the energy function with respect to time:

$$\begin{aligned}\dot{Q} &\leq (a_{max} - \alpha \|\bar{L}(t_{n-1}) + H(t_{n-1})\|_1) \|\tilde{v}\|_1 \\ &\leq (a_{max} - \alpha \cdot \min \|\bar{L}(t_{n-1}) + H(t_{n-1})\|_1) \|\tilde{v}\|_1 \\ &\leq (a_{max} - 2\alpha) \|\tilde{v}\|_1 \\ &\leq 0, \forall t \in [t_{n-1}, t_n].\end{aligned}\quad (59)$$

Hence,  $\forall t \in [t_{n-1}, t_n]$ , the energy function follows that:

$$Q(t_n) \leq Q(t_{n-1}) \leq Q_{max}, \quad (60)$$

which means that when the multi-vehicle system switches the network topology, the control protocol can still ensure that there will be no collision. Hence, the vehicle will not exceed the road boundary and will not collide with the HVs. In addition, according to the definition of control connection topology  $\mathcal{G}(t)$ , when the system switches the control connection topology, although the original control connections may disappear, new control connections will be generated to ensure the connectivity of the whole system.

Similarly, at any time  $t_n$  of control connection topology switching, the number of control connections in the new topology  $\mathcal{G}(t_n)$  is always limited, and the range of its number also satisfies (57). We define a following set:

$$S = \{\tilde{r} \in D_1, \tilde{v} \in \mathbb{R}^{2N} | Q(\tilde{r}, \tilde{v}) \leq Q_{max}\}, \quad (61)$$

$$\text{where } D_1 = \left\{ \tilde{r} = \mathbb{R}^{N^2} | \|\tilde{r}_i - \tilde{r}_j\|_2 \in [0, V_{ij}^{-1}(Q_{max})] \right\}_{\forall(i, j) \in \mathcal{G}(t_n)}.$$

According to LaSalle's invariance principle, state trajectory of this multi-vehicles system will converge to the following set:

$$S_{\text{end}} = \{\tilde{r} \in D_1, \tilde{v} \in \mathbb{R}^{2N} | \dot{Q}(\tilde{r}, \tilde{v}) = 0\}. \quad (62)$$

Therefore, when the multi-vehicle system enters steady state, we can get  $\dot{Q}(\tilde{r}, \tilde{v}) = 0$ . According to the (59), we can calculate :  $\|\tilde{v}\|_1 = 0$ , which means the velocity of the follower vehicles will eventually synchronize with the leader AV. Moreover, for each  $\mathcal{G}(t_n)$ , all the follower vehicles will form a connected traffic flow with the leader AV.

#### IV. EXPERIMENTS

In this section, we verify the effectiveness of the proposed algorithm through a very representative overtaking scenario. Unreal Engine and Matlab are used in the simulation experiments. Unreal Engine is a powerful game physics engine that can be used to build very realistic autopilot scenarios that are closer to real-world driving environments. Matlab is used for algorithm development. Through the combination of Unreal Engine and Matlab, the overtaking scene of the autonomous driving team can be simulated more realistically and the overtaking process can be observed more intuitively.

##### A. Parameters and variables setting

As for the motion planning algorithm of leader AV, we set the following experimental parameters and variables (shown as Table I).

$$\begin{aligned}\dot{Q}(\tilde{r}, \tilde{v}) &= \sum_{i=1}^N \tilde{v}_i^T \alpha \sum_{j \in \mathcal{N}_i} \bar{a}_{ij} \left\{ \text{sgn} \left[ \sum_{p \in \mathcal{N}_j} \bar{a}_{jp} (\tilde{v}_j - \tilde{v}_p) + h_j \tilde{v}_j \right] \right\} \\ &\quad - \sum_{i=1}^N \tilde{v}_i^T \alpha \sum_{j \in \mathcal{N}_i} \bar{a}_{ij} \left\{ \text{sgn} \left[ \sum_{p \in \mathcal{N}_i} \bar{a}_{ip} (\tilde{v}_i - \tilde{v}_p) + h_i \tilde{v}_i \right] \right\} - \sum_{i=1}^N \tilde{v}_i^T \dot{v}_l \\ &= -\alpha \tilde{v}^T (\bar{L}(t_0) + H(t_0)) \text{sgn} [\bar{L}(t_0) + H(t_0) \tilde{v}] - \sum_{i=1}^N \tilde{v}_i^T \dot{v}_l \leq \|\dot{v}_l\|_1 \|\tilde{v}\|_1 - \alpha \|\bar{L}(t_0) + H(t_0)\|_1 \|\tilde{v}\|_1 \\ &\leq (a_{max} - \alpha \|\bar{L}(t_0) + H(t_0)\|_1) \|\tilde{v}\|_1 \leq (a_{max} - \alpha \cdot \min \|\bar{L}(t_0) + H(t_0)\|_1) \|\tilde{v}\|_1.\end{aligned}\quad (55)$$

TABLE I: Simulation parameters and variables of motion planning algorithm of leader AV

Parameter and variable names	Value
Initial position of Leader	(12, -2.875) m
Initial velocity of Leader	5 m/s
Initial acceleration of Leader	0 m/s <sup>2</sup>
Initial position of human-operated vehicle	(32, -3) m
Initial velocity of human-operated vehicle	10 m/s
Initial acceleration of human-operated vehicle	0.1 m/s <sup>2</sup>
The jerk of human-operated vehicle	0.01 m/s <sup>3</sup>
Attractive force gain ( $K_p, K_v, K_a$ )	(500,2000,2000)
Repulsive force gain of vehicles ( $\eta_p, \eta_v$ )	(100, 200)
Repulsive force gain of road boundary	4000
Mass of Leader	1000 kg
Sampling time	0.1 s
Maximum velocity in longitudinal	33 m/s
Maximum velocity in lateral	5 m/s
Maximum acceleration in longitudinal	5 m/s <sup>2</sup>
Maximum acceleration in lateral	1.3 m/s <sup>2</sup>

For the distributed control topology, We set the following simulation conditions:

- Assume that the velocity of all vehicles are randomly selected in [0, 33] m/s .
- In order to reflect the complete lane change and overtaking process, we assume that the AV fleet and the human-operated vehicle are in the same initial lane.
- The maximum acceleration of the vehicle is 5 m/s<sup>2</sup>. According to the conditions of distributed control protocol, we set control gain  $\alpha = 5 > \frac{a_{max}}{2}$ .
- Vehicle-to-vehicle topology connection communication range is 8 m.
- The desired distance of the vehicle in the longitudinal direction and lateral direction are, respectively, 6 m and 0 m .
- The minimum distance allowed between the vehicle  $i$  and the road boundary or obstacles  $d_{ek} = 1$ .

We add an additive hysteresis constant  $\varepsilon_0$  to all potential field functions to prevent vehicle connection topology disconnection in discrete time domain. Hence,  $V_{max}(\|r_{ij}\|) = V_{r_{ij}}(R - \varepsilon_0)$ .  $V_{max}(\|r_{ik}\|) = V_{r_{ik}}(\varepsilon_0)$ .  $V_{max}(\|r_{en}\|) = V_{r_{en}}(\varepsilon_0)$ .  $V_{max}(\|r_{il}\|) = V_{r_{il}}(R_l - \varepsilon_0)$ . According to (49),  $Q_{max}$  can be calculated as:

$$\begin{aligned} Q_{max} \leq & \frac{N(N-1)}{2} V_{r_{ij}}(R - \varepsilon_0) + MNV_{max} V_{r_{ik}}(\varepsilon_0) \\ & + NV_{r_{en}}(\varepsilon_0) + NV_{r_{il}}(R_l - \varepsilon_0) \\ & + \frac{N}{2}(v_{max}^T v_{max}). \end{aligned} \quad (63)$$

Here, we set  $N = 2$ , and  $\varepsilon_0 = 0.5$ .  $Q_{max}$  can be determined by the upper bound of the vehicle velocity. It is calculated that:  $Q_{max} \leq 1153$ .  $c_1 = c_2 = c_3 = c_4 = 50$ . Substituting the parameters into (50), we can obtain the specific form of the interaction potential function.

## B. Results and analysis

1) *Overtaking performance*: In this scenario, the leader AV needs to complete the planning of overtaking trajectory and

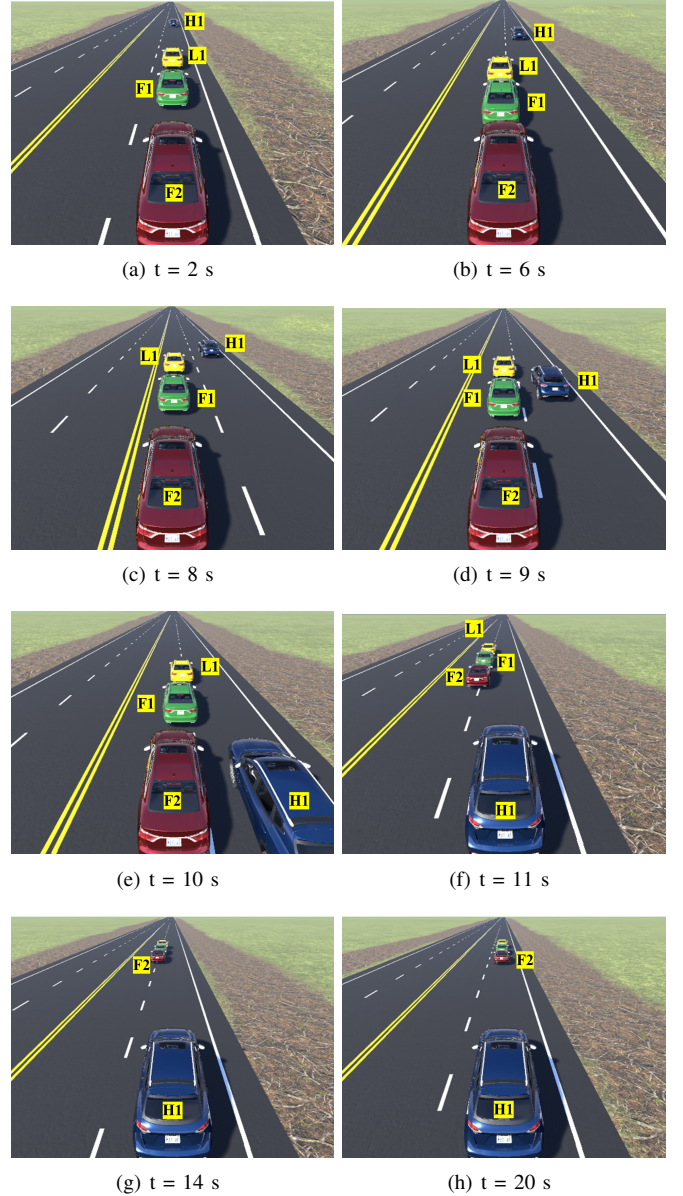


Fig. 6: The process of lane changing and overtaking in Unreal Engine. H1 denotes the human-operated vehicle. L1, F1, and F2, respectively, denote the leader AV, first follower AV, and second follower AV.

lead the follower AVs to complete the overtaking of human-driven vehicles in front. The follower AVs need to track the leader AV and maintain a safe distance from other vehicles. We simulated the overtaking scenario with Unreal Engine. In this engine, we can clearly observe the detailed process of the overtaking of the AV fleet . Fig. 6 shows the process of autonomous overtaking and lane changing of the AV fleet. At  $t = 2$  s, the AV fleet and the H1 were in the same lane. When  $t = 6$  s, the AV fleet was in the process of lane changing, from the right lane to the left lane. After the AV fleet finished lane changing, it began to approach and overtook the H1 (as shown in Fig. 6(c)). At  $t = 9$  s, the AV fleet began to accelerate to overtake the H1 on the right lane. By  $t = 10$  s, the L1 and F1

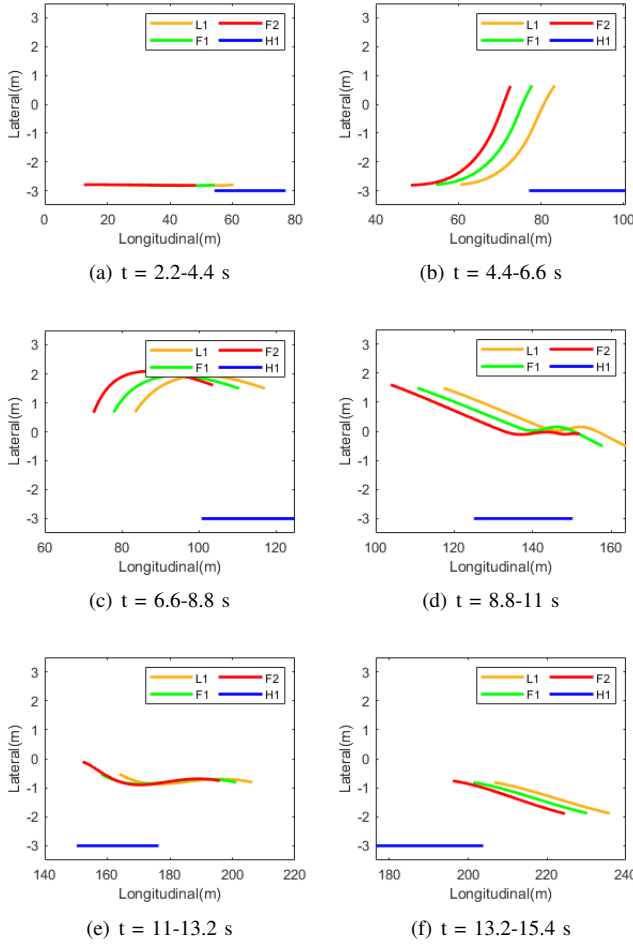


Fig. 7: Detailed autonomous overtaking process of autonomous vehicles fleet with one leader AV

completely overtook the H1. In Fig. 6(f), the whole AV fleet completed the overtaking and began to switch to the initial lane. Then, the vehicle returned to the initial lane at  $t = 20$  s and the overtaking and lane changing process were finished. During the whole overtaking process, there was no collision and no driving out of the road boundary. The corresponding motion trajectory can be clearly shown in Fig. 7. It can be seen that in the process of overtaking and lane changing, the trajectories of the all AVs are smooth. In particular, in Fig. 7(d) and (e), the trajectories of F1 and F2 show lateral fluctuations, which is the obstacle avoidance behavior of vehicles. After completing obstacle avoidance, F1 and F2 can still follow the leader AV. It shows that in the control protocol designed in this paper, human-operated vehicle will not cut off the connection topology of the AV fleet.

We discuss the leader VA's motion planning algorithm in this paper independently. Fig. 8 is the position and velocity curve of the leader AV. As can be seen from the figure, the lateral and longitudinal velocity of the vehicle converge to the same value as the velocity of the HV. The position difference between the leader AV and the HV converges to a constant value. This constant position difference is given by the vehicle's decision module, and this constant position

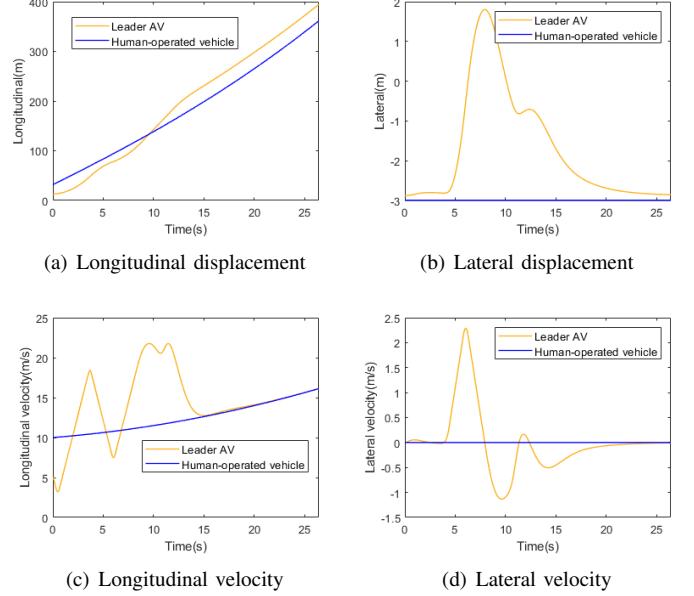
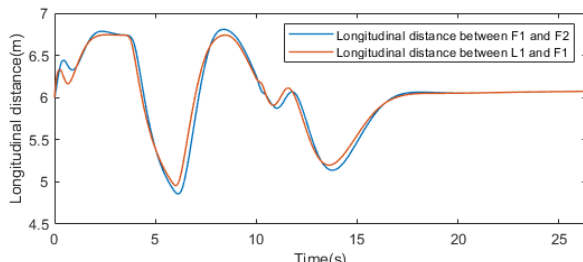


Fig. 8: The displacement and velocity curves of leader AV and human-operated vehicle

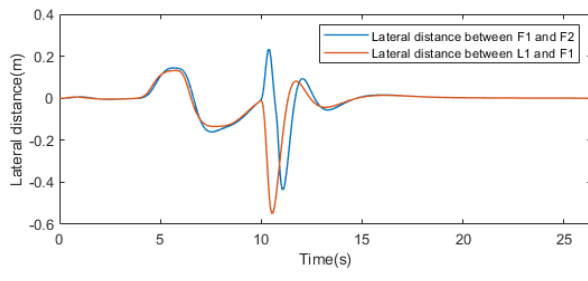
difference will be adjusted according to the size of the fleet.

Fig. 9 and Fig. 10, respectively, represent the position difference and speed difference curves between AV fleet member F1, F2, and L1. In the longitudinal direction, the distance between vehicles fluctuate greatly in the process of overtaking. However, this fluctuation does not cause collisions between vehicles, nor does it sever the topological connection between vehicles. After overtaking, the distance between vehicles converges to an expected value. In the lateral direction, similar results can be achieved. As for the velocity difference, in the process of lane changing and overtaking, the velocity difference between vehicles changes dramatically. This is caused by the AV's autonomous obstacle avoidance. After overtaking, the velocity difference between vehicles converges to zero, which means that the velocity of the whole AV fleet is synchronized.

**2) Robustness verification:** We verify the robustness of the algorithm by randomly setting the speed of H1 and the initial speed of the AV fleet members. The rest of the simulation settings remain the same as Table I. Therefore, we defined three different cases, including Case-1 where the initial velocities of F1, F2, L1, and H1 are 1 m/s, 2 m/s, 5 m/s, and 10 m/s, Case-2 where the initial velocities of F1, F2, L1, and H1 are 1 m/s, 2 m/s, 4 m/s, and 7 m/s, and Case-3 where the initial velocities of F1, F2, L1, and H1 are 2 m/s, 3 m/s, 6 m/s, and 9 m/s. As illustrated in Fig. 11, the automatic overtaking was completed at different initial speeds for both AVs and H1. Additionally, in real-world applications, the information obtained via V2V is not completely accurate. Similar to [54], we assume that both the position, velocity and acceleration information obtained from each V2V communication is subject to a random error which ranges from -3% to 3%. We additionally run the simulation experiment with simulation settings in Table I and obtain the

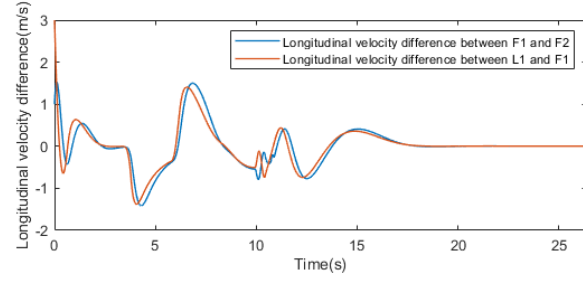


(a) Longitudinal distance

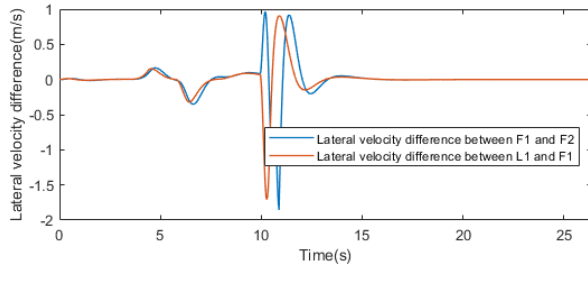


(b) Lateral distance

Fig. 9: The displacement distance curve between the members of the autonomous vehicles fleet



(a) Longitudinal velocity difference

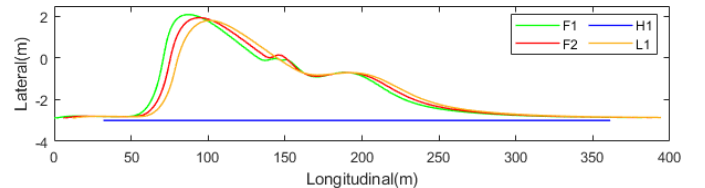


(b) Lateral velocity difference

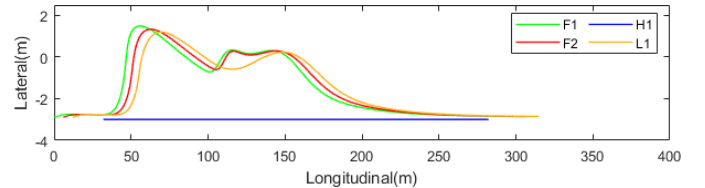
Fig. 10: The velocity difference curve between the members of the autonomous vehicle fleet

results considering V2V communication errors. As depicted in Fig. 12, after adding the random communication error, the trajectory of the AV fleet shifts slightly compared to Fig. 11(a). As a result, the overtaking and lane changing are completed safely, which shows that the proposed algorithm is robust in the presence of communication errors.

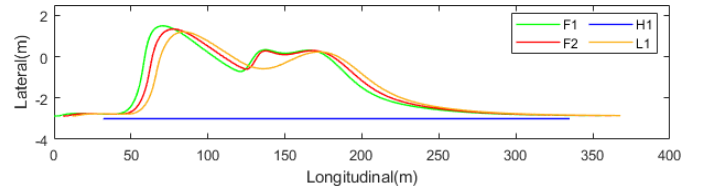
3) Comparison: There are many studies on overtaking of AV, e.g., [42] proposes a probability-based approach in the background of the graph-based route selection optimization,



(a) Case1: the initial velocities of F1, F2, L1, and H1 are 1 m/s, 2 m/s, 5 m/s, and 10 m/s, respectively.



(b) Case2: the initial velocities of F1, F2, L1, and H1 are 1 m/s, 2 m/s, 4 m/s, and 7 m/s, respectively.



(c) Case3: the initial velocities of F1, F2, L1, and H1 are 2 m/s, 3 m/s, 6 m/s, and 9 m/s, respectively.

Fig. 11: The process of overtaking and changing lanes of AV fleet in different cases.

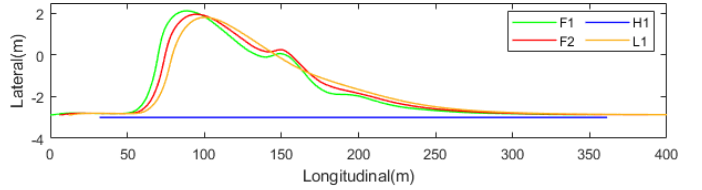


Fig. 12: The result shows the trajectory of the AV fleet when V2V communication has a random error of 3%. The initial velocities of F1, F2, L1, and H1 are 1 m/s, 2 m/s, 5 m/s, and 10 m/s, respectively.

with which the motions of the HVs are predicted. This study considers HVs and aims to search for an overtaking path with the lowest collision probability through the probability distribution of vehicle speed and acceleration. However, this method is only applicable to individual vehicle overtaking and not to multi-vehicle systems, as the method does not require cooperative control between AVs. In our proposed control strategy, not only HVs are considered, but also a cooperative control protocol is designed to ensure a multi-vehicle system with good group performance. In [29], a novel swarm intelligence-based algorithm is proposed for producing the multi-objective optimal overtaking trajectory of autonomous ground vehicles, which obtains good overtaking and obstacle avoidance trajectories. However, this approach is still not applicable to multi-vehicle systems. Moreover, in this study, the object to be overtaken is modeled as a static obstacle. Therefore the validity of the method for dynamic HVs is not

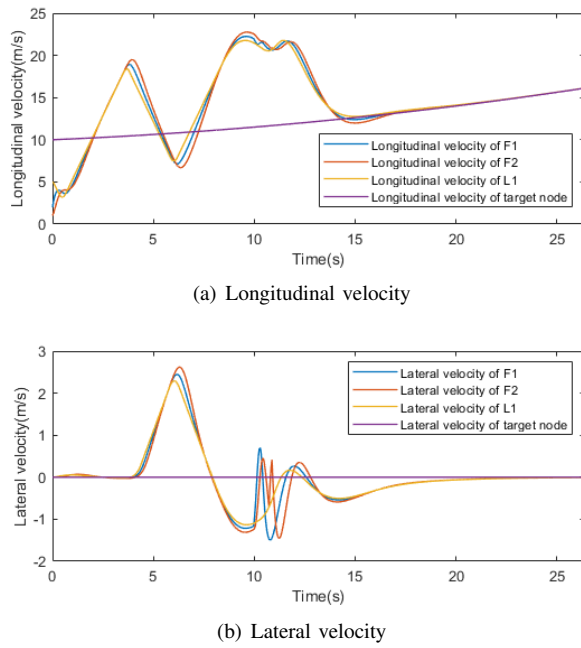


Fig. 13: Velocity curves of AV fleet members and target node

guaranteed. In our overtaking control strategy, we consider HVs while focusing on the cooperative control of multi-vehicle systems, which enables the vehicle platoon to complete safe overtaking while ensuring the stability of the platoon. In this paper, the overtaking problem of multi-vehicle system is transformed into a dynamic target tracking problem of multi-agent system. A similar study has also conducted in [55], which a distributed control framework is used to dynamically track wildfire spreading by drones. However, based on this strategy, the speeds of drones cannot be synchronized with the spread of dynamic wildfires. In our study, speed synchronization of multi-agent with dynamic target is realized. In Fig. 13, velocity curves for target node and all AV fleet members are displayed. For a dynamic target node with varying acceleration, the leader AV and the followers can accurately track the dynamic target node and achieve speed synchronization. This is due to the utilization of the proposed control strategy, where the leader AV uses a separate motion planning algorithm and the rest of the followers use a distributed cluster control. Under this strategy, each follower does not need to be equipped with an acceleration sensor. It is only the leader AV which gets the acceleration information of the HV. This greatly reduces the cost of hardware implementation and communication. As the bounded distributed control protocol is used in this paper, the control output of the follower vehicle is bounded, which is very beneficial to the application of the algorithm in real-world scenarios.

## V. CONCLUSION

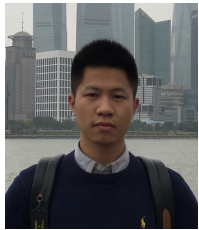
This paper addresses the distributed motion control problem of autonomous vehicles operating in a complex multi-lane, heterogeneous vehicle platoon. The proposed algorithm also includes an effective mechanism for safe autonomous overtaking when the platoon consists of autonomous and human-

operated vehicles. This paper introduces the Velocity Difference Potential Field (VDPF) and Acceleration Difference Potential Field (ADPF) techniques, which are the improved versions of the conventional Artificial Potential Field (APF) method. The overtaking problem of the unmanned vehicles in a multi-lane platoon has been formulated as a formation tracking problem, in which the human-operated vehicles are set as targets. The proposed technique can effectively handle situations where the acceleration of a leader vehicle changes suddenly due to approaching an obstacle or the neighboring vehicles. It also ensures that the follower unmanned vehicles achieve speed synchronization with the leader vehicle having variable acceleration. In addition, the follower vehicles of the platoon also avoid obstacles while complying with the desired formation tracking objectives. The paper has used Matlab and Unreal Engine software simulation platforms to test the usefulness and feasibility of the proposed algorithm. The simulation results show that a group of autonomous vehicles operate safely in a complex, heterogeneous multi-lane platoon, exhibiting safe overtaking, changing lanes, obstacle avoidance and dynamic target tracking. To further increase the comfort of the proposed method, optimization-based techniques may need to be integrated in the protocol design, which will be explored in our future works.

## REFERENCES

- [1] W. H. Organization *et al.*, “Global status report on road safety 2018: Summary,” World Health Organization, Tech. Rep., 2018.
- [2] U. Montanaro, S. Dixit, S. Fallah, M. Dianati, A. Stevens, D. Oxtoby, and A. Mouzakitis, “Towards connected autonomous driving: review of use-cases,” *Vehicle System Dynamics*, vol. 57, no. 6, pp. 779–814, 2019.
- [3] A. Eskandarian, *Handbook of intelligent vehicles*. Springer, 2012, vol. 2.
- [4] S. Singh, “Critical reasons for crashes investigated in the national motor vehicle crash causation survey,” Tech. Rep., 2015.
- [5] W. Payre, J. Cestac, and P. Delhomme, “Intention to use a fully automated car: Attitudes and a priori acceptability,” *Transportation Research Part F: Traffic Psychology and Behaviour*, vol. 27, pp. 252–263, 2014.
- [6] D. Rojas-Rueda, M. J. Nieuwenhuijsen, H. Khreis, and H. Frumkin, “Autonomous vehicles and public health,” *Annual Review of Public Health*, vol. 41, pp. 329–345, 2020.
- [7] D. A. Rozemond, “Using intelligent agents for pro-active, real-time urban intersection control,” *European Journal of Operational Research*, vol. 131, no. 2, pp. 293–301, 2001.
- [8] D. González, J. Pérez, V. Milanés, and F. Nashashibi, “A review of motion planning techniques for automated vehicles,” *IEEE Transactions on Intelligent Transportation Systems*, vol. 17, no. 4, pp. 1135–1145, 2015.
- [9] A. Haydari and Y. Yilmaz, “Deep reinforcement learning for intelligent transportation systems: A survey,” *IEEE Transactions on Intelligent Transportation Systems*, vol. 23, no. 1, pp. 11–32, 2022.
- [10] J. Hu, A. E. Turgut, B. Lennox, and F. Arvin, “Robust formation coordination of robot swarms with nonlinear dynamics and unknown disturbances: Design and experiments,” *IEEE Transactions on Circuits and Systems II: Express Briefs*, vol. 69, no. 1, pp. 114–118, 2022.
- [11] J. Jiang and A. Astolfi, “Lateral control of an autonomous vehicle,” *IEEE Transactions on Intelligent Vehicles*, vol. 3, no. 2, pp. 228–237, 2018.
- [12] H. Zhu, K.-V. Yuen, L. Mihaylova, and H. Leung, “Overview of environment perception for intelligent vehicles,” *IEEE Transactions on Intelligent Transportation Systems*, vol. 18, no. 10, pp. 2584–2601, 2017.
- [13] J. Hu, P. Bhownick, F. Arvin, A. Lanzon, and B. Lennox, “Cooperative control of heterogeneous connected vehicle platoons: An adaptive leader-following approach,” *IEEE Robotics and Automation Letters*, vol. 5, no. 2, pp. 977–984, 2020.

- [14] B. Wu, L. Qian, M. Lu, D. Qiu, and H. Liang, "Optimal control problem of multi-vehicle cooperative autonomous parking trajectory planning in a connected vehicle environment," *IET Intelligent Transport Systems*, vol. 13, no. 11, pp. 1677–1685, 2019.
- [15] J. Hu, B. Lennox, and F. Arvin, "Robust formation control for networked robotic systems using negative imaginary dynamics," *Automatica*, vol. 140, p. 110235, 2022.
- [16] S. Xie, J. Hu, Z. Ding, and F. Arvin, "Collaborative overtaking of multi-vehicle systems in dynamic environments: A distributed artificial potential field approach," in *2021 20th International Conference on Advanced Robotics (ICAR)*, 2021, pp. 873–878.
- [17] J. Hu, P. Bhowmick, I. Jang, F. Arvin, and A. Lanzon, "A decentralized cluster formation containment framework for multirobot systems," *IEEE Transactions on Robotics*, vol. 37, no. 6, pp. 1936–1955, 2021.
- [18] Y. Liu and R. Bucknall, "A survey of formation control and motion planning of multiple unmanned vehicles," *Robotica*, vol. 36, no. 7, pp. 1019–1047, 2018.
- [19] K. Wu, J. Hu, Z. Ding, and F. Arvin, "Mixed controller design for multi-vehicle formation based on edge and bearing measurements," in *2022 20th European Control Conference (ECC)*, 2022.
- [20] B. Wang, H. Ashrafiou, and S. Nersesov, "Leader-follower formation stabilization and tracking control for heterogeneous planar underactuated vehicle networks," *Systems & Control Letters*, vol. 156, p. 105008, 2021.
- [21] J. Hu, H. Niu, J. Carrasco, B. Lennox, and F. Arvin, "Fault-tolerant cooperative navigation of networked uav swarms for forest fire monitoring," *Aerospace Science and Technology*, vol. 123, p. 107494, 2022.
- [22] M. Goli and A. Eskandarian, "A nonlinear model predictive control design for autonomous multivehicle merging into platoons," *SAE International Journal of Transportation Safety*, vol. 10, no. 09-10-01-0004, 2021.
- [23] ———, "Merging strategies, trajectory planning and controls for platoon of connected, and autonomous vehicles," *International Journal of Intelligent Transportation Systems Research*, vol. 18, no. 1, pp. 153–173, 2020.
- [24] S. Dixit, U. Montanaro, M. Dianati, D. Oxtoby, T. Mizutani, A. Mouzakitis, and S. Fallah, "Trajectory planning for autonomous high-speed overtaking in structured environments using robust mpc," *IEEE Transactions on Intelligent Transportation Systems*, vol. 21, no. 6, pp. 2310–2323, 2019.
- [25] S. Dixit, S. Fallah, U. Montanaro, M. Dianati, A. Stevens, F. McCullough, and A. Mouzakitis, "Trajectory planning and tracking for autonomous overtaking: State-of-the-art and future prospects," *Annual Reviews in Control*, vol. 45, pp. 76–86, 2018.
- [26] B. Németh, P. Gáspár, and T. Hegedűs, "Optimal control of overtaking maneuver for intelligent vehicles," *Journal of Advanced Transportation*, vol. 2018, 2018.
- [27] J. Karlsson, N. Murgovski, and J. Sjöberg, "Computationally efficient autonomous overtaking on highways," *IEEE Transactions on Intelligent Transportation Systems*, vol. 21, no. 8, pp. 3169–3183, 2019.
- [28] R. Deng, B. Di, and L. Song, "Cooperative collision avoidance for overtaking maneuvers in cellular v2x-based autonomous driving," *IEEE Transactions on Vehicular Technology*, vol. 68, no. 5, pp. 4434–4446, 2019.
- [29] R. Chai, A. Tsourdos, A. Savvaris, S. Chai, Y. Xia, and C. L. Philip Chen, "Multiobjective overtaking maneuver planning for autonomous ground vehicles," *IEEE Transactions on Cybernetics*, vol. 51, no. 8, pp. 4035–4049, 2021.
- [30] U. S. Ghumman, F. Kunwar, B. Benhabib *et al.*, *Guidance-based online motion planning for autonomous highway overtaking*. University of Toronto, 2008, [Ph.D. thesis].
- [31] J. Li, M. Ran, and L. Xie, "Design and experimental evaluation of a hierarchical controller for an autonomous ground vehicle with large uncertainties," *IEEE Transactions on Control Systems Technology*, pp. 1–13, 2021.
- [32] R. Lattarulo, D. He, and J. Pérez, "A linear model predictive planning approach for overtaking manoeuvres under possible collision circumstances," in *2018 IEEE Intelligent Vehicles Symposium (IV)*, 2018, pp. 1340–1345.
- [33] C. Burger and M. Lauer, "Cooperative multiple vehicle trajectory planning using miqp," in *2018 21st International Conference on Intelligent Transportation Systems (ITSC)*, 2018, pp. 602–607.
- [34] J. Li, M. Ran, and L. Xie, "Efficient trajectory planning for multiple non-holonomic mobile robots via prioritized trajectory optimization," *IEEE Robotics and Automation Letters*, vol. 6, no. 2, pp. 405–412, 2020.
- [35] Y. Kuwata, J. Teo, G. Fiore, S. Karaman, E. Frazzoli, and J. P. How, "Real-time motion planning with applications to autonomous urban driving," *IEEE Transactions on Control Systems Technology*, vol. 17, no. 5, pp. 1105–1118, 2009.
- [36] L. Labakhua, U. Nunes, R. Rodrigues, and F. S. Leite, "Smooth trajectory planning for fully automated passengers vehicles: Spline and clothoid based methods and its simulation," in *Informatics in Control Automation and Robotics*, 2008, pp. 169–182.
- [37] M. Kaushik, N. Singhania, and K. M. Krishna, "Parameter sharing reinforcement learning architecture for multi agent driving," in *Proceedings of the Advances in Robotics*, 2019, pp. 1–7.
- [38] M. Kaushik, V. Prasad, K. M. Krishna, and B. Ravindran, "Overtaking maneuvers in simulated highway driving using deep reinforcement learning," in *2018 IEEE Intelligent Vehicles Symposium (IV)*, 2018, pp. 1885–1890.
- [39] X. Li, X. Qiu, J. Wang, and Y. Shen, "A deep reinforcement learning based approach for autonomous overtaking," in *IEEE International Conference on Communications Workshops (ICC Workshops)*, 2020, pp. 1–5.
- [40] L. Yu, X. Shao, and X. Yan, "Autonomous overtaking decision making of driverless bus based on deep q-learning method," in *IEEE International Conference on Robotics and Biomimetics (ROBIO)*, 2017, pp. 2267–2272.
- [41] S. Na, H. Niu, B. Lennox, and F. Arvin, "Bio-inspired collision avoidance in swarm systems via deep reinforcement learning," *IEEE Transactions on Vehicular Technology*, vol. 71, no. 3, pp. 2511–2526, 2022.
- [42] T. Hegedűs, B. Németh, and P. Gáspár, "Graph-based multi-vehicle overtaking strategy for autonomous vehicles," *IFAC-PapersOnLine*, vol. 52, no. 5, pp. 372–377, 2019.
- [43] B. Németh, T. Hegedűs, and P. Gáspár, "Model predictive control design for overtaking maneuvers for multi-vehicle scenarios," in *18th European Control Conference (ECC)*, 2019, pp. 744–749.
- [44] I. B. Viana, H. Kanchwala, K. Ahiska, and N. Aouf, "A comparison of trajectory planning and control frameworks for cooperative autonomous driving," *Journal of Dynamic Systems, Measurement, and Control*, vol. 143, no. 7, p. 071002, 2021.
- [45] I. B. Viana and N. Aouf, "Distributed cooperative path-planning for autonomous vehicles integrating human driver trajectories," in *International Conference on Intelligent Systems (IS)*, 2018, pp. 655–661.
- [46] M. Kneissl, A. K. Madhusudhanan, A. Molin, H. Esen, and S. Hirche, "A multi-vehicle control framework with application to automated valet parking," *IEEE Transactions on Intelligent Transportation Systems*, vol. 22, no. 9, pp. 5697–5707, 2021.
- [47] J. Karlsson, C.-I. Vasile, J. Tumova, S. Karaman, and D. Rus, "Multi-vehicle motion planning for social optimal mobility-on-demand," in *IEEE International Conference on Robotics and Automation (ICRA)*, 2018, pp. 7298–7305.
- [48] J. Harding, G. Powell, R. Yoon, J. Fikentscher, C. Doyle, D. Sade, M. Lukuc, J. Simons, J. Wang *et al.*, "Vehicle-to-vehicle communications: readiness of V2V technology for application." United States. National Highway Traffic Safety Administration, Tech. Rep., 2014.
- [49] F. Bounini, D. Gingras, H. Pollart, and D. Gruyer, "Modified artificial potential field method for online path planning applications," in *IEEE Intelligent Vehicles Symposium (IV)*, 2017, pp. 180–185.
- [50] Y. Wang, Q. Shao, J. Zhou, H. Zheng, and H. Chen, "Longitudinal and lateral control of autonomous vehicles in multi-vehicle driving environments," *IET Intelligent Transport Systems*, vol. 14, no. 8, pp. 924–935, 2020.
- [51] I. Bae, J. Moon, H. Park, J. H. Kim, and S. Kim, "Path generation and tracking based on a bezier curve for a steering rate controller of autonomous vehicles," in *16th International IEEE Conference on Intelligent Transportation Systems (ITSC)*, 2013, pp. 436–441.
- [52] F. Chen, Y. Cao, and W. Ren, "Distributed average tracking of multiple time-varying reference signals with bounded derivatives," *IEEE Transactions on Automatic Control*, vol. 57, no. 12, pp. 3169–3174, 2012.
- [53] C. Jie, *Collaborative clustering motion control for multi-agent systems*. Science Press, 2017.
- [54] H. Haes Alhelou, M. E. H. Golshan, and N. D. Hatzigaryiou, "A decentralized functional observer based optimal lfc considering unknown inputs, uncertainties, and cyber-attacks," *IEEE Transactions on Power Systems*, vol. 34, no. 6, pp. 4408–4417, 2019.
- [55] H. X. Pham, H. M. La, D. Feil-Seifer, and M. C. Deans, "A distributed control framework of multiple unmanned aerial vehicles for dynamic wildfire tracking," *IEEE Transactions on Systems, Man, and Cybernetics: Systems*, vol. 50, no. 4, pp. 1537–1548, 2018.



**Songtao Xie** received B.Eng degree in Mechanical design as well as manufacturing and its automation from Sichuan University, Chengdu, China, in 2016 and Master degree in Mechanical Engineering Design from the University of Manchester, U.K. in 2017. He worked as a function and system development engineer in GEELY AUTOMOBILE HOLDINGS LIMITED from 2017 to 2019. Now, he is a Ph.D candidate in University of Manchester. His research interests include multi-agent, distributed control, and autonomous driving.



**Farshad Arvin** received the BSc degree in Computer Engineering, the MSc degree in Computer Systems engineering, and the PhD degree in Computer Science, in 2004, 2010, and 2015, respectively. Farshad is an Associate Professor in Robotics in the Department of Computer Science at Durham University in UK. Prior to that, he was a Senior Lecturer in Robotics at The University of Manchester, UK. He visited several leading institutes including Artificial Life Laboratory with the University of Graz, Institute of Microelectronics, Tsinghua University, Beijing, and Italian Institute of Technology (iit) in Genoa as a Senior Visiting Research Scholar. His research interests include swarm robotics and autonomous multi-agent systems. He is the Founding Director of the Swarm & Computation Intelligence Laboratory (SwaCIL) formed in 2018.



**Junyan Hu** received B.Eng degree in Automation from Hefei University of Technology in 2015 and Ph.D degree in Electrical and Electronic Engineering from the University of Manchester in 2020.

Junyan is an Assistant Professor in Robotics with the Department of Computer Science, University College London (UCL). Prior to joining UCL, he worked as a Research Associate in Robotics at the University of Manchester. His research interests include swarm intelligence, multi-agent systems, cooperative navigation, distributed control, and their applications in autonomous driving and robotics. He has been serving as a reviewer for many top/leading international journals and conferences in the field of robotics and artificial intelligence. He is a Member of IEEE CSS Technical Committee on Manufacturing Automation and Robotic Control, IEEE RAS Technical Committee on Multi-Robot Systems, and IFAC Technical Committee on Mechatronic Systems.



**Parijat Bhownick** received his B. Tech degree in Electrical Engineering from West Bengal University of Technology, Kolkata, India in 2008 and received his M.E. degree in Control Systems Engineering from Jadavpur University, Kolkata, India in 2012. He has completed his Ph.D. degree in Control Engineering from Indian Institute of Technology Kharagpur, India, in 2018. He is currently an Assistant Professor at Indian Institute of Technology, Guwahati. He worked as a Post-doctoral Research Associate at the University of Manchester from 2018 to 2021.

His research interests include robust control of negative-imaginary systems, passivity-based control and decentralized integral control.



**Zhengtao Ding** received the B.Eng. degree from Tsinghua University, Beijing, China, in 1984, and the M.Sc. degree in systems and control, and the Ph.D. degree in control systems from the University of Manchester Institute of Science and Technology, Manchester, U.K. in 1986 and 1989, respectively. After working as a Lecturer with Ngee Ann Polytechnic, Singapore, for ten years, he joined the University of Manchester in 2003, where he is currently Professor of Control Systems with the Dept of Electrical and Electronic Engineering. He is the author

of the book: Nonlinear and Adaptive Control Systems (IET, 2013) and has published over 300 research articles. His research interests include nonlinear and adaptive control theory and their applications, more recently network-based control, distributed optimization and distributed machine learning, with applications to power systems and robotics. Prof. Ding has served as an Associate Editor for the IEEE Transactions on Automatic Control, IEEE Control Systems Letters, and several other journals. He is a member of IEEE Technical Committee on Nonlinear Systems and Control, IEEE Technical Committee on Intelligent Control, and IFAC Technical Committee on Adaptive and Learning Systems.